THE INTEGRATION OF MULTIPLE CARDIOVASCULAR AND PULMONARY MODELS INTO A SINGLE UNIFIED CARDIOPULMONARY MODEL

A Thesis
Submitted to the Graduate Faculty
of the
North Dakota State University
of Agriculture and Applied Science

By

Julian Earl Thrash III

In Partial Fulfillment of the Requirements
for the Degree of
MASTER OF SCIENCE

Major Program:
Electrical and Computer Engineering

April 2024

Fargo, North Dakota

North Dakota State University
Graduate School

Title

The Integration of Multiple Cardiovascular and Pulmonary Models into a Single Unified Cardiopulmonary Model

By

Julian Earl Thrash III

The Supervisory Committee certifies that this ***disquisition*** complies with North Dakota State University's regulations and meets the accepted standards for the degree of

MASTER OF SCIENCE

SUPERVISORY COMMITTEE:

Dr. Daniel Ewert
Chair

Dr. Lawrence Mulligan

Dr. Benjamin Braaten

Dr. Amanda Brooks

Approved:

April 8, 2024
Date

Dr. Benjamin Braaten
Department Chair

ABSTRACT

There has been an increasing effort to employ cardiovascular (CV) and pulmonary models to assist in the study of disease, answer research questions, and study the effects of a medical treatment or device. To properly study the intricate dynamics of the CV and pulmonary systems, a comprehensive model is required to achieve a holistic understanding of its mechanics and view the emergent properties of the complex and dynamic cardiopulmonary system. This study builds on the work of Mauro Ursino et al., by taking their multiple CV and pulmonary models and integrating them together within the scalable environment of MATLAB and Simulink. Multiple published mathematical models were implemented and integrated together within Simulink and MATLAB, its hemodynamics and lung mechanics were verified, and the model was additionally adapted for use simulating an invasive pressure-volume (PV) study of the effects of vascular aging of the aorta on cardiac function and efficiency.

ACKNOWLEDGEMENTS

I want to thank my parents, sister, and family for their support and care over the years as I persevered through both my Bachelor's and Master's degrees in Electrical and Computer Engineering. Thank you Dr. Ewert and Dr. Braaten for your support and guidance during my transition in my field of study as well as giving me the chance to work on a project and area of study that I'm very passionate about. Thank you, Dr. Mulligan and Dr. Ewert, for your guidance and help improving my understanding of cardiac physiology and for giving me the opportunity to begin developing my career through the research projects and papers we've published together. Thank you, Dr. Brooks, for your support in the early days of my graduate research and helping to foster a love of research and motivating me to go into graduate school. Through the work on this thesis and in the graduate courses I've taken with my committee, I feel that I've greatly grown as an engineer and gotten the chance to work on research that I wanted to do since the start of collage. I look forward to further growing in my skills during my PhD studies with you all.

DEDICATION

I want to dedicate this to my mother and father Janet and Julian Thrash; my little sister Josselyn Thrash; my Aunt Karen Nickel; my maternal grandparents Frank and Judy Nickel; my paternal grandparents Bill and Betty Thrash; and the rest of my family. Thank you, Grandpa Frank Nickel and papa Bill Thrash who encouraged me to become an engineer through the projects we did together. I know you're both watching over me every day.

TABLE OF CONTENTS

LIST OF TABLES

Table Page

LIST OF FIGURES

LIST OF ABBREVIATIONS

ANS.....Autonomic Nervous System

BP.....Arterial Blood Pressure

C_A.....Aortic Arch Compliance

CO_2.....Carbon Dioxide

Cp,equivalent .....Equivalent Compliance of the Arteries

CV.....Cardiovascular

DBP.....Diastolic Blood Pressure of the Systemic Arteries

dP/dt.....Derivative of Left Ventricular Pressure

dP/dtmax.....Maximum Value of dLVP/dt

$dP/dt_{max\text{-}EDV}$.....Preload Adjusted dP/dtmax

EDPVR.....End-Diastolic Pressure Volume Relation

EDV.....End Diastolic Volume of the Left Ventricle

EDV-PVA.....Preload Adjusted Pressure Volume Area

ESPVR.....End-Systolic Pressure Volume Relation

LVEDP.....Left Ventricular End-Diastolic Pressure

LVP.....Left Ventricular Pressure

LVV.....Left Ventricular Volume

MAP.....Mean Arterial Blood Pressure

MAP.....Mean Arterial Blood Pressure

MSE.....Mean Squared Error

O_2.....Oxygen

ODE.....Ordinary Differential Equation

Pes.....End Systolic Pressure of the Left Ventricle

Pla/LAP.....Left Atrial Pressure

PP .....Pulse Pressure

Ppa/PAP .....Pulmonary Artery Pressure

PRSW.....Preload Recruitable Stroke Work

PV .....Pressure-Volume

PVA.....Pressure Volume Area

RAP.....Right Atrial Pressure

RT .....Total Peripheral Resistance

RVP.....Right Ventricular Pressure

RVV .....Right Ventricular Volume

S.M. .....Simulink Cardiopulmonary Model

SBP .....Systolic Blood Pressure of the Systemic Arteries

SV .....Stroke Volume

SVl .....Left Ventricular Stroke Volume

SVr .....Right Ventricular Stroke Volume

SW.....Stroke Work

VA.....Vascular Aging

VCO .....Vena Caval Occlusion

VCP.....Vena Caval Pressure

LIST OF APPENDIX TABLES

1. INTRODUCTION

There has been an increasing effort to develop cardiovascular (CV) and pulmonary models to simulate the effects of disease, study the impact of medical device therapies, and predict the impact of CV or pulmonary-related diseases on patient health. Most research focuses on designing multi-scale or multi-dimensional models that rigorously calculate the dynamics of select regions of the cardiopulmonary system (Niederer et al., 2019). However, the complexity and interlinked mechanics of the system require a holistic model approach to simulate physiologic data accurately. The key physiological attributes that define the cardiopulmonary system's function include the hemodynamic vascular system, blood-tissue gas exchange, lung mechanics, respiratory-gas exchange, and the heart and the myocardium under the control of the autonomic nervous system (ANS) (John, 2011). A model with these elements is required to 1) evaluate research questions that are not feasible in animal or human subjects, 2) plan pre-clinical studies, 3) validate and test medical devices, 4) train machine learning algorithms, or 5) aid in medical diagnosis and treatment (Asai et al., 2021; Zieliński et al., 2022).

The foundational work in mathematical modeling of the cardiovascular and pulmonary system started with the work done by Otto Frank, modeling the dynamics of an arterial system using a pressure generation source connected to an elastance and peripheral resistance element to study fluid flow called the Windkessel(Frank, 1899, 1990). Grodins built on this work and began viewing the system as a steady-state feedback-regulated closed "circuit" system (Grodins, 1959). Guyton et al. built on this work by creating an expansive circulatory, respiratory, endocrine, gas-exchange, renal, metabolic, and ANS control of heart rate, stroke volume, and vessel dilation (Guyton et al., 1972). The major obstacles of this accumulated work were the limited computational power of the time, the steady-state modeling of system dynamics rather than an

integrated dynamic approach and missing or incomplete knowledge of elements of the cardiopulmonary system that developed after decades of subsequent research.

Mauro Ursino and his colleagues completed the research and mathematical modeling of many vital systems needed for a comprehensive cardiopulmonary model (Albanese et al., 2016; Magosso & Ursino, 2001; Ursino, 1998; Ursino & Magosso, 2000, 2002). Each model was designed and verified to recreate key mechanisms of cardiovascular function and control under normal systemic conditions. One of their primary research goals was to utilize their computational models to study the physiological response to changing levels of oxygen and carbon dioxide blood-gas concentrations within the body by tuning their parameters to recreate severe conditions such as hypoxia and hypercapnia. The primary limitations of the extensive work completed by Ursino et al. were the multiple versions of models designed for unique research scenarios and their focus on validating and tuning their models for extreme oxygen and carbon dioxide blood-gas concentration levels. Nevertheless, the scope of their work in developing multiple lumped-parameter cardiovascular and pulmonary models has significantly advanced cardiopulmonary computational modeling research. Despite these accomplishments, integrating these multiple models into a single unified model of the cardiopulmonary system is required to advance the field of human physiological simulation, the design and testing of medical devices, and aid in diagnosing and treating patients. To further their work, this thesis aims to integrate the various models of Ursino et al. within the scalable program development environment of MATLAB and Simulink, recreate their published model results, and begin furthering the work by tuning model parameters and modifying the cardiac system equations to create a cardiac system capable of producing physiologic pressure-volume (PV) waveforms for use as a research tool simulating invasive studies of the cardiovascular system.

In chapter two, the thesis will discuss the methods of integrating the various Ursino models into the MATLAB/Simulink environment and the model modification for normal physiology. Next, the third chapter will discuss the process of verifying the combined Simulink model using published waveform datapoints to determine the accuracy and correlation of model-generated results to the original works of Ursino. The fourth chapter will discuss the validation of the Simulink model, starting with the modification made to the cardiac system, the simulation of an invasive PV loop study examining the effects of vascular aging (VA) on cardiovascular performance and efficiency, and then discuss the results and findings published from the study (Mulligan, Mitrev, et al., 2024; Mulligan et al., 2023; Mulligan, Ungerleider, et al., 2024). Finally, the fifth chapter will discuss the work, the limitations of the Simulink model, future directions for this research, and conclude.

2. METHODS AND MODEL DEVELOPMENT

2.1. Methods Overview and Goals

This chapter will discuss the decision to use the MATLAB/Simulink environment for model integration and development, implementing and unifying multiple CV and pulmonary models, and then integrating and testing systems. The first contribution of this work began with integrating multiple Ursino cardiovascular and pulmonary mathematical models in MATLAB and Simulink to create a single computational model. This thesis's second and major goal was to modify the cardiac system to simulate invasive PV studies and begin improving the cardiovascular system, as outlined in chapter four. This chapter will outline the process of implementing these contributions and the physiological and engineering theory that went into this work.

2.2. Selection of the MATLAB/Simulink Development Environment

The unified cardiopulmonary model development utilized the MATLAB/Simulink environment because it could represent complex and interlinked feedback-regulated systems, integrate additional subsystems within a scalable integrated development environment, and the multiple toolboxes that facilitated testing. A significant benefit of Simulink is its ability to represent complex control systems in a visually interconnected manner, inspect elements, and record data(MathWorks, 2024). This feature, matched with the capabilities of MATLAB for data processing and code integration within the Simulink model, greatly assisted in achieving both contributions for this work. The nature of the cardiopulmonary system and the multiple Ursino models necessitated having a platform that allowed additional subsystems to be added and debug the closed-loop feedback system(MathWorks, 2024). Other systems with calculations that vary during the step computation of the model created system memory feedback or read-after-write

errors called algebraic loops(MathWorks, 2023). Debugging these memory issues used Simulink code advisory and algebraic loop detection tools. The features and resources within the MATLAB/Simulink environment were pivotal to achieving both the goals and contributions of this thesis work.

2.3. The Development of a Unified Cardiopulmonary Model Based on the Work of Ursino

2.3.1. Overview of the Unified Cardiopulmonary Model

Integrating multiple cardiovascular and pulmonary models designed by Ursino et al. involved a process of taking multiple systems from each model, modeling equations within Simulink, identifying their connections with other systems, correlating parameters of equations with other models, and performing integration and testing of closed-loop systems. The systems represented in the combined model included: 1) the left and right side of the heart, 2) systemic circulation through five vascular compartments, 3) tissue gas exchange, 4) venous gas transport, 5) local-effect autoregulation, 6) lung mechanics, 7) pulmonary hemodynamic circulation, 8) lung-gas exchange, and 9) ANS stimulation and regulation. Each system consists of multiple linked phenomenological or constitutive equations representing the biological, chemical, or physics mechanics of a system using differential equations. Ursino et al. developed many models by reworking previous system equations or adding new subsystems to meet the needs of a specific research application(Albanese et al., 2016; Magosso & Ursino, 2001; Ursino, 1998; Ursino & Magosso, 2000, 2002). The iterative nature of developing each model meant that there were versions of systems with different input/output behavior, varied naming schemes for the solved quantities, and parameters with unique names and values that posed a challenge with integrating them into a single unified cardiopulmonary model in Simulink. Integrating models involved taking a system and programming its equations in Simulink and MATLAB, identifying

any model changes to equations and parameters that altered functionality, and then using some test input to verify the function of a system. The Simulink program used an ode23t solver, which computes ordinary differential equations within continuous time by taking a variable timestep trapezoid approximation of an integral. When two different sets of equations are linked together, such as in an ordinary differential equation (ODE), the feedback and feedthrough of different quantities in the system can create instability. Integrating systems of multiple linked equations required an iterative sensitivity integration process to connect major systems and account for negative feedback regulation, computational integration or differentiation errors, algebraic loops, startup parameter value errors, and identifying instability regions within equations in Simulink. This section will outline the integration of each system from Ursino's CV and pulmonary models within Simulink as well as the sensitivity integration process.

2.3.2. The Heart

The left and right sides of the heart act as the driving force of circulation throughout the human body, which Ursino modeled using an electrical analog hemodynamic system (Ursino, 1998). The subsystems of the heart consist of the right atrium (Figure 2.1, label 1), right ventricle (Figure 2.1, label 2), pulmonary valve (Figure 2.1, label 3), left atrium (Figure 2.1, label 4), left ventricle (Figure 2.1, label 5), and aortic valve (Figure 2.1, label 6) modeled using multiple hemodynamic equations. Implementation followed the process of loading deoxygenated blood into the right side of the heart, flowing through the different regions, and unloading newly reoxygenated blood at the output of the left side of the heart. Inputs into the heart are the systemic venous return of blood (F_{ra} is equivalent to Q_{tv}), the deoxygenated concentration of blood from the venous pool gas transport ($C_{v,\,gas}$), and ANS stimulation from the sympathetic (f_{sh}) and parasympathetic (f_{ev}) systems (Figure 2.1, label 8), each of which connects to the left

and right ventricle subsystems. Hemodynamic and blood-gas concentration inputs are transferred to the right ventricle (F_{ir}) and pumped into the pulmonary circulatory system (F_{or}) for reoxygenation (Figure 2.1, label 7). The outputs of the pulmonary circulation, oxygenated arterial blood-gas concentrations ($C_{a,\ gas}$), and partial pressures ($P_{a,\ gas}$) are transported via the hemodynamics of the pulmonary vein (Q_{pv} is equivalent to F_{la}) to connect with the left atrium, which fills the left ventricle (F_{il}) which subsequently contracts and ejects blood through the aortic valve (F_{ol}) (Albanese et al., 2016; Ursino, 1998).

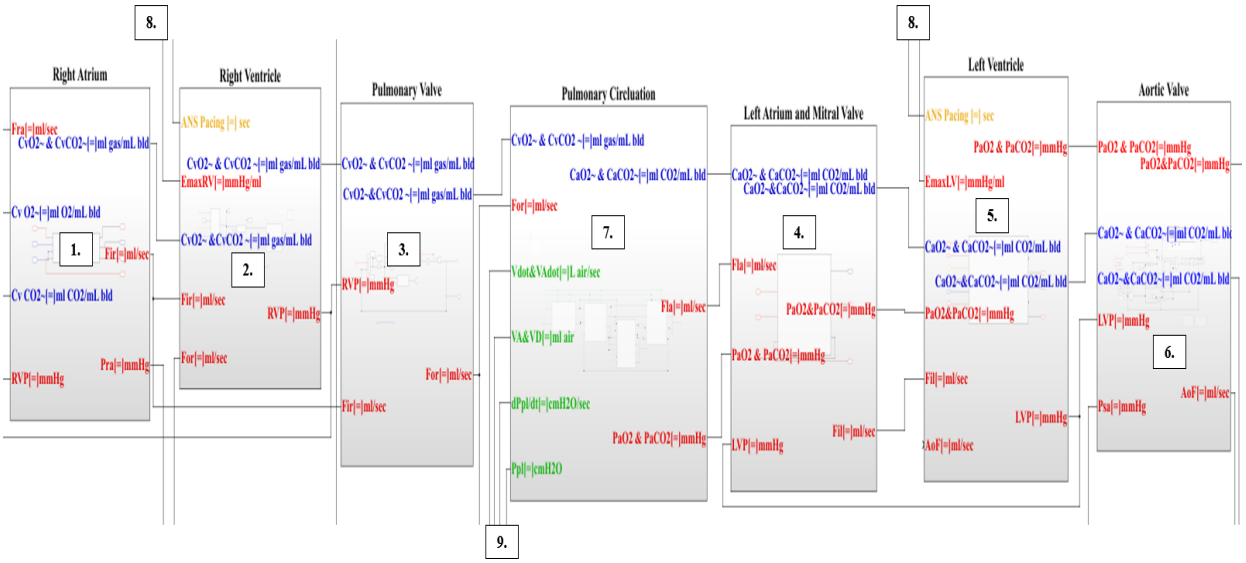

Figure 2.1: Right and Left Heart Connected with Pulmonary Circulation, Lung Mechanics, and ANS

(Label Key: Red = Hemodynamic Signal; Blue = Blood Gas Concentration; Yellow = ANS Innervation; Green = Respiratory Mechanics; Pink = Gas Fraction/Saturation)

2.3.3. Systemic Vascular Circulation System

Blood circulation throughout the human body starts at the aortic arch and splits along parallel vascular pathways that supply oxygen and nutrients for normal metabolic function. Mauro Ursino modeled systemic vascular circulation using an electrical analog hemodynamic model starting with the flow of blood out of the aortic valve (F_{ol}), which enters the arch region where the systemic arterial pressure (P_{sa}) drives blood flow (F_{sa}) into a parallel circuit containing

the coronary, brain, skeletal muscle, splanchnic, and extra-splanchnic vascular compartments (denoted by 'j'), each branch consisting of an arterial region (represented by subscript 'p') and a venous section (designated by subscript 'v') (Albanese et al., 2016). Implementation of systemic circulation equations began with the calculation of the systemic arterial hemodynamics (Figure 2.2, label 1) based on inflow exiting the heart (F_{ol}), which connects to a parallel arterial pressure ($P_{arterial}$) calculation for each vascular branch (Figure 2.2, label 2) that divides blood flow to the five vascular compartments (Figure 2.2, labels 3 to 12). Next, the computed regional hemodynamics of each arterial (p) and venous (v) region drive oxygenated blood gas concentrations ($C_{a,\,gas}$) to the tissue gas exchange and waste ($C_{v,\,gas}$) to the venous pool gas transport, respectively. Finally, the venous blood flow of each branch combines at the thoracic veins (Q_{tv} is equivalent to F_{ra}), which generates a pressure (P_{tv}) consisting of the transmural pressure of the thoracic veins ($P_{tm,\,tv}$) combined with the pleural cavity pressure (P_{pl}) that influence the venous region hemodynamics and blood flow to the right atrium (F_{ra}) (Figure 2.2 label 13).

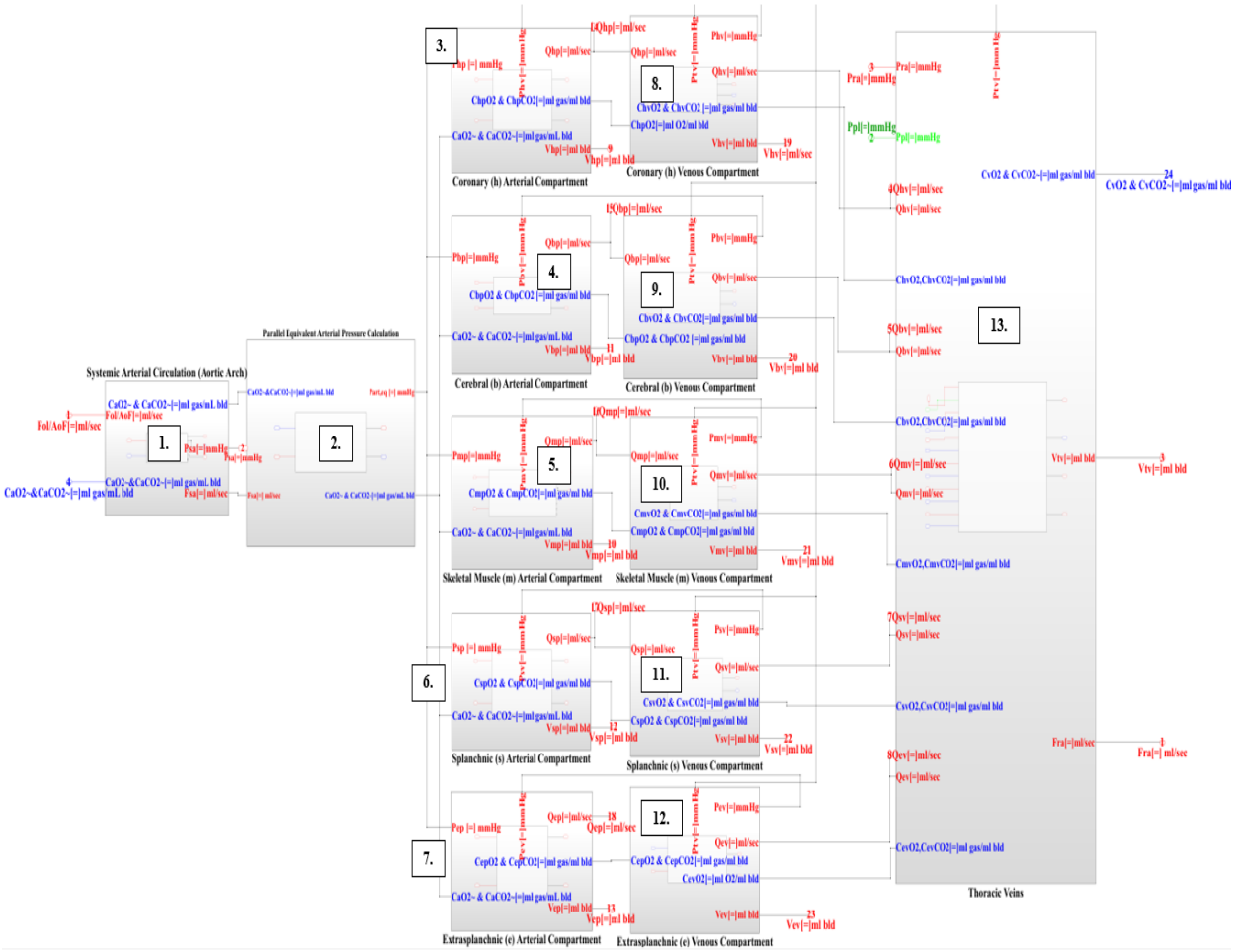

Figure 2.2: Systemic Circulation of Five Parallel Vascular Compartments

2.3.4. Tissue Gas Exchange

The exchange of oxygen from the arterial blood ($C_{a,\,O2}$) and nutrients is vital for metabolism and normal systemic function of the body's tissues. Ursino represented this exchange mechanism by using a mass-flow balance model that determines the concentration of consumed oxygen ($C_{jp,\,O2}$) and produced carbon dioxide ($C_{jp,\,CO2}$) based on the arterial blood flow (Q_{jp}) and the constant rate of blood-gas consumption/production ($M_{O2,\,jp}$ and $M_{CO2,\,jp}$, respectively) in each compartment (Albanese et al., 2016). Implementing this system involved representing each tissue gas exchange equation for a given vascular region (Figure 2.3 labels 1 through 5) in parallel with the arterial hemodynamics (Q_{jp}) and directly inputting the total blood-gas concentration of

arterial oxygen ($C_{a,\,O2}$) and carbon dioxide ($C_{a,\,CO2}$) within the blood. A given blood volume in an arterial region (V_{jp}) determines the total arterial blood-gas concentration for its respective compartment ($C_{jp,\,gas}$). This system is directly inputted into Ursino's venous gas transport model to determine the final blood-gas concentrations of oxygen and carbon dioxide carried to the lungs.

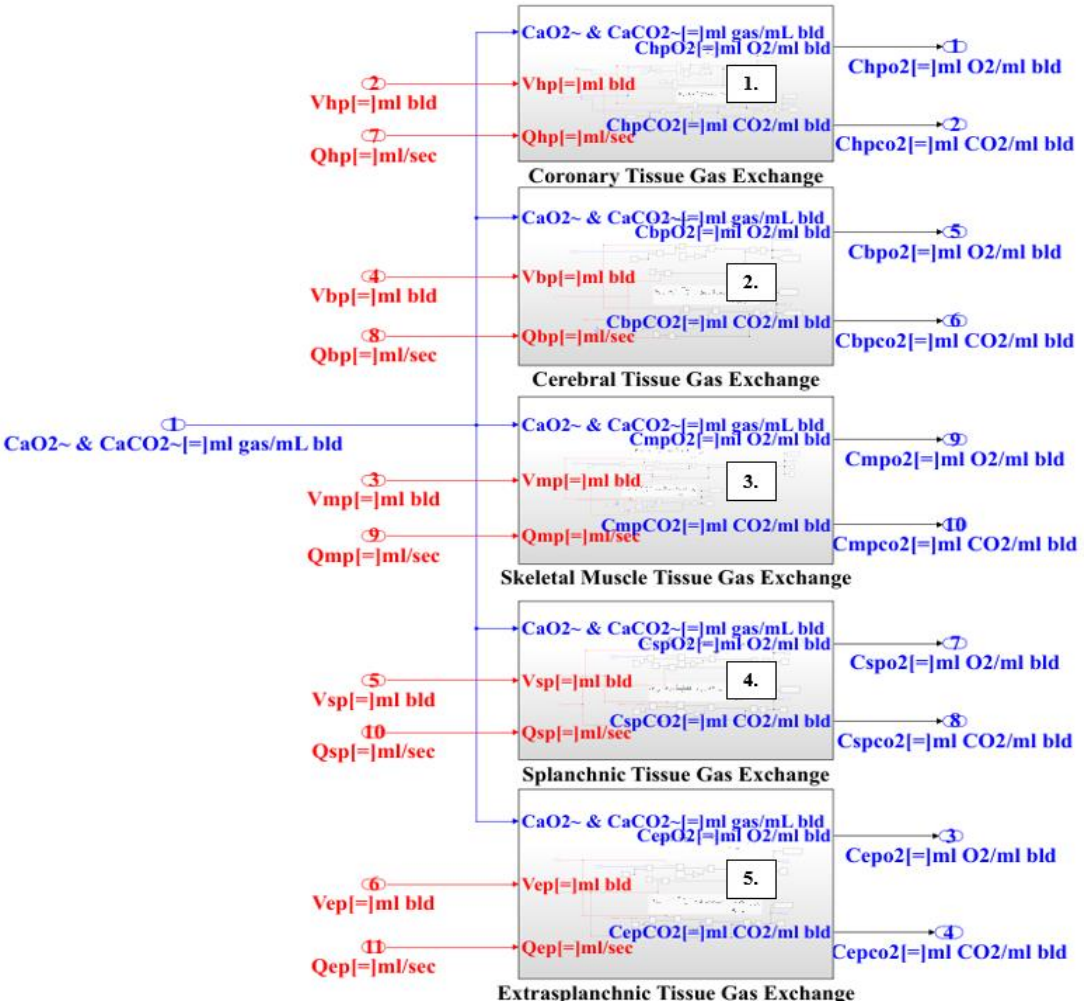

Figure 2.3: Tissue Gas Exchange

2.3.5. Venous Pool Gas Transport

Blood-gas exchange and metabolic activity within the tissues lower the oxygen concentration and increase waste carbon dioxide affixed to the volumes of blood in the veins.

Ursino et al. represented this process of calculating the total concentrations of gasses ($C_{jv,\,gas}$) in the venous blood of each vascular compartment (V_{jv}) in a mass-flow balance equation system and then pooling the gas concentrations together ($C_{v,\,O2}$ and $C_{v,\,CO2}$) at the thoracic veins (Q_{tv}) for transport to the right side of the heart (F_{ra}). System implementation involved representing each venous compartment as a subsystem (Figure 2.4 labels 1-5) containing the blood-gas concentration equations ($C_{jv,\,gas}$) and operating in parallel with the hemodynamics of each compartment's veins. Each venous compartment blood-gas oxygen and carbon dioxide concentration was then fed into their respective mass pool equations (Figure 2.4 labels 6) to calculate $C_{v,\,O2}$ and $C_{v,\,CO2}$. Each venous compartment's blood-gas concentrations are summated and transported via the combined hemodynamics of the venous system, which transports the deoxygenated blood to the right atrium (F_{ra}) and eventually to the respiratory system (F_{pa}). The delay in gases affixed to the blood is represented by a Simulink time delay ($\widetilde{C_{v,O2}}$ and $\widetilde{C_{v,CO2}}$) representing the time to take a blood concentration to the respiratory system, using parameters derived from the published work of Ursino et al. (Albanese et al., 2016).

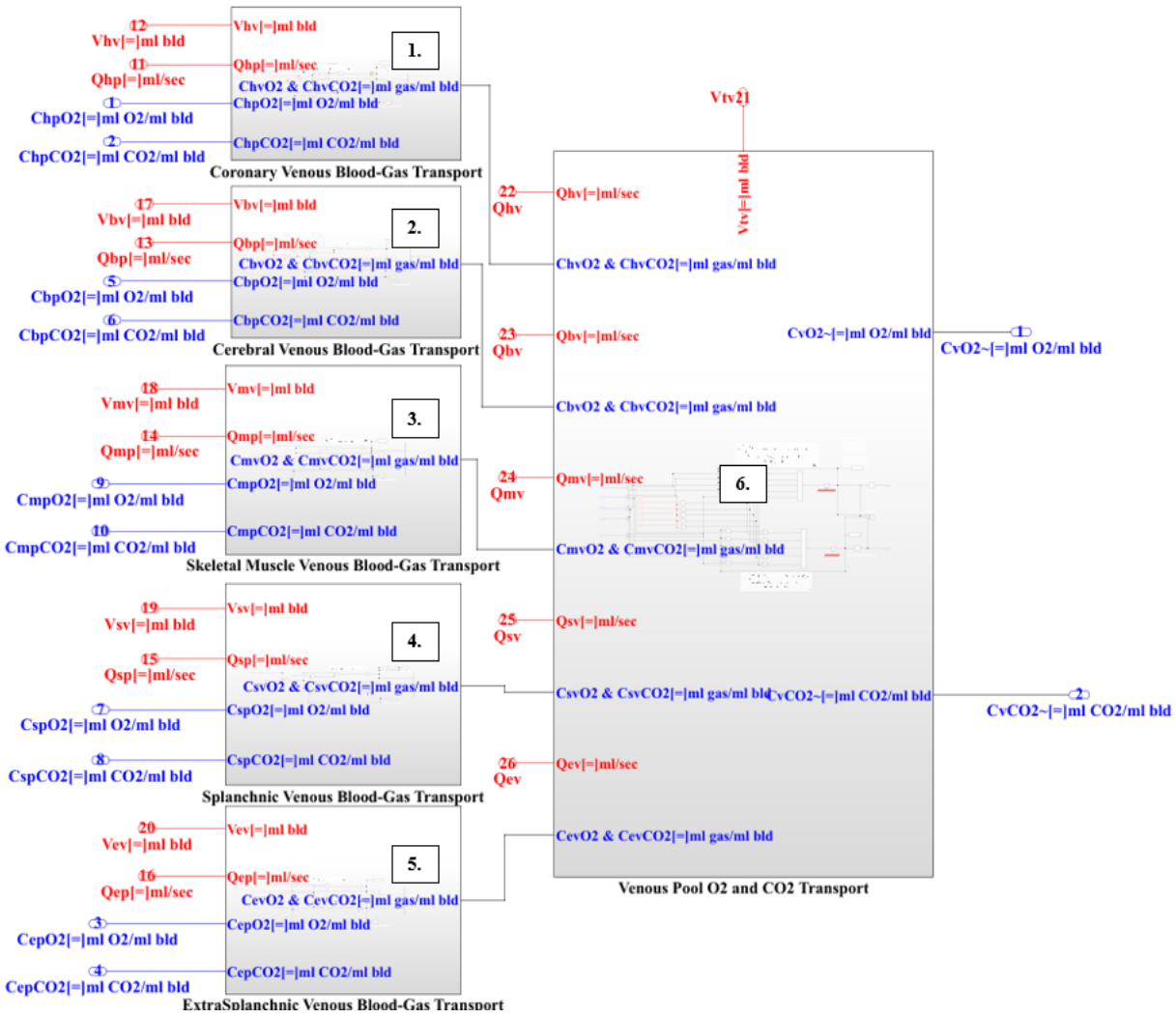

Figure 2.4: Venous Gas Transport

2.3.6. Local Effect Autoregulation

Vessel resistance regulates the hemodynamics of the arterial system by constricting or relaxing in diameter depending on ANS stimulation or by the local effect of blood-gas concentration of a vascular compartment. Ursino et al. modeled the localized automatic regulation of resistance for the coronary (h), cerebral (b), and skeletal muscle (m) arteries as multistage ODE equations based on venous oxygen blood-gas concentrations in each vascular region(Magosso & Ursino, 2001; Ursino & Magosso, 2000). Each autoregulated resistance compares the instantaneous venous oxygen concentration ($C_{jv,\,O2}$) to a nominal level($C_{jv,\,O2n}$)

(Figure 2.5 labels 1 to 3), calculates a response (x_{jp}) via an ODE (Figure 2.5 labels 4 to 6), and then determines the final arterial resistance (R_{jp}) using the nominal resistance ($R_{jp,\,n}$) and dynamic response (x_{jp}). Skeletal muscle arterial resistance differs in that it incorporates a nominal resistance set point ($R_{mp,\,n}$) that dynamically varies due to ANS stimulation (f_{sp}) to represent the shifting hemodynamic response in the muscles due to varied levels of work (Figure 2.5 label 6)(Ursino & Magosso, 2000). These resistances directly output to the arterial system equations for the coronary (R_{hp}), cerebral (R_{bp}), and skeletal muscle (R_{mp}) to regulate the regional hemodynamics of their respective vascular branch by dilating under low oxygen blood-gas concentrations and constricting under high concentrations.

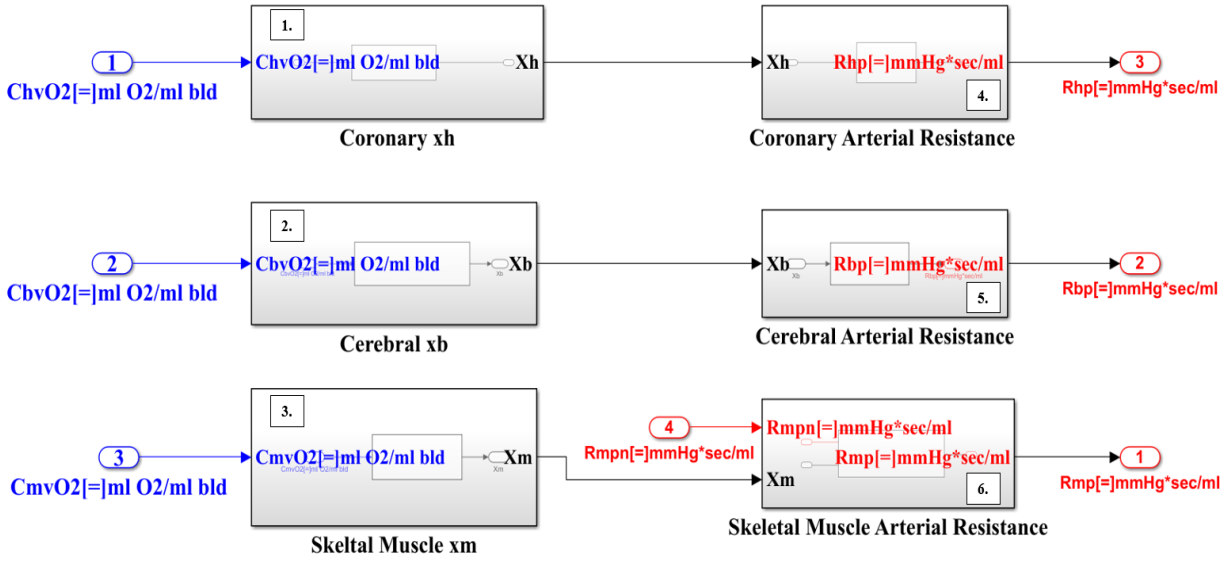

Figure 2.5: Local Effect Autoregulation

2.3.7. Lung Mechanics

Mechanical pumping of the lungs drives lung-gas exchange and influences the hemodynamics of the cardiovascular system via the inhalation and exhalation of the respiratory muscles. Ursino modeled lung mechanics using a multistage electrical circuit model that represents the total flow of air ($\dot{V}$) through the open airway (ao), larynx (l), trachea (tr), the

bronchial tubes (b), and then down to the alveolar sacs (A)(Albanese et al., 2016). Each region of the pulmonary circuit contains an air pressure (P_l, P_{tr}, P_b, P_A), resistance (R_l, R_{tr}, R_b, R_A), and a reservoir containing volumes of air within its compliant regions (V_l, V_{tr}, V_b, V_A) that each dictates the total airflow through the respiratory system ($\dot{V}$) and to the site of gas exchange in the alveolar sacs ($\dot{V}_A$) (Albanese et al., 2016). Implementing these equations began with the respiratory muscle pressures, Pmus and Ppl, that drive inhalation and exhalation based on an ANS-stimulated negative pressure process (Figure 2.6, label 1). Next, these pressures connect in parallel with the trachea (Figure 2.6, label 3), bronchial tubes (Figure 2.6, label 4), and alveolar sacs (Figure 2.6, label 5) to compute their mechanical air pressure and volume. The larynx (Figure 2.6, label 2) and open airway region (Figure 2.6, label 9) connect with the parallel regions to complete the circuit system. The total instantaneous flow of air ($\dot{V}$) (Figure 2.6, label 6) through the respiratory circuit, airflow through the alveolar sacs ($\dot{V}_A$) (Figure 2.6, label 7), total air volume within the lungs (V_L) and non-exchanging dead space (V_D) are computed (Figure 2.6, label 8) and drive lung-gas exchange.

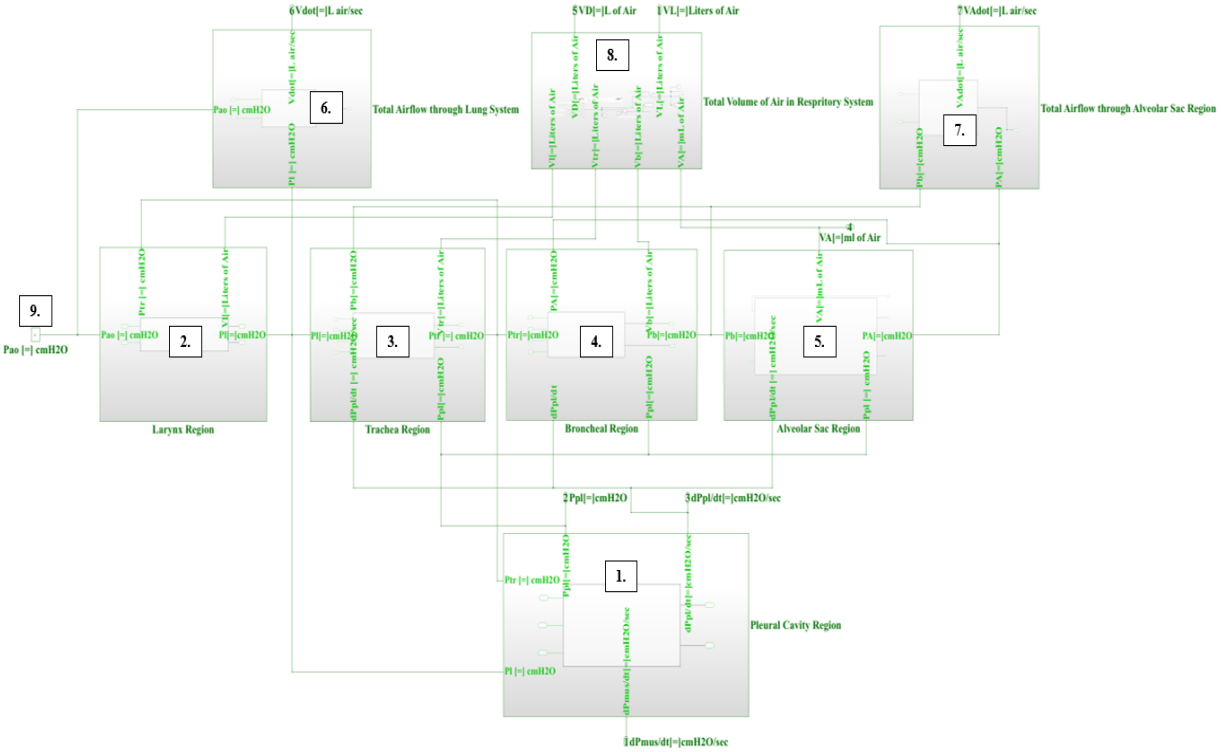

Figure 2.6: Lung Mechanics

2.3.8. Pulmonary Circulation

The pulmonary circulation system carries deoxygenated blood pumped by the right ventricle to the alveolar capillaries for blood-gas exchange, which is then reoxygenated and carried to the left atrium. Ursino et al. represented pulmonary circulation using an electrical analog containing a pulmonary arterial (pa) region that divides into two parallel pathways: the flow through the peripheral alveolar capillaries (pp), the non-exchanged blood located in the pulmonary shunt (ps) and the mixing of reoxygenated and shunted blood that occurs at the pulmonary vein (pv) which connects to the left atrium (Albanese et al., 2016; Ursino, 1998; Ursino & Magosso, 2000). Modeling pulmonary circulation started with its artery hemodynamic equations, which carry the time-delayed concentrations of venous blood ($\widetilde{C_{v,O2}}$ and $\widetilde{C_{v,CO2}}$) and are driven by the pleural cavity pressure (P_{pl}) (Figure 2.7, label 1) and the flow of blood ejected

out the right ventricle into the pulmonary arteries (Q_{pa}) (Figure 2.7, label 2). Blood flow through the pulmonary artery connects to the parallel pulmonary capillaries (pp) and shunt (ps) compartments (Figure 2.7, label 3), each containing equations that compute the hemodynamics of blood volumes that will exchange their blood-gas concentrations in the lungs and the shunted portion (Figure 2.7, label 4). Blood flow from the capillaries (Q_{pp}) and shunt (Q_{ps}) combine at the pulmonary vein compartment (Figure 2.7, label 5), which computes the dynamics of the reoxygenated blood ($\widetilde{C_{a,O2}}$ *and* $\widetilde{C_{a,CO2}}$) transported to the left atrium (Q_{pv} is equivalent to Q_{la}) (Figure 2.7, label 5).

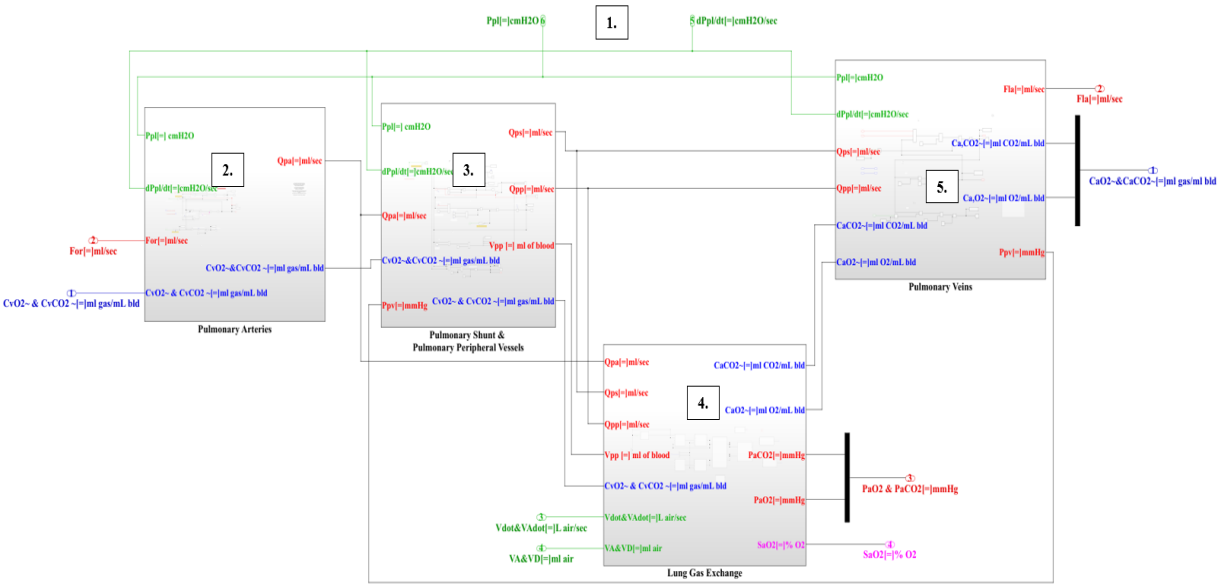

Figure 2.7: Pulmonary Circulation and Lung Gas Exchange

2.3.9. Lung Gas Exchange

The lung gas exchange system removes waste carbon dioxide blood-gas concentrations ($\widetilde{C_{v,O2}}$ and $\widetilde{C_{v,CO2}}$) from venous blood flow to the pulmonary capillaries (Q_{pp}) that connect to the alveolar sacs. A dissociation process removes carbon dioxide from the hemoglobin and affixes oxygen concentrations to the blood ($C_{a,\,O2,}$ and $C_{a,\,CO2}$) which will reoxygenate the systemic

tissues. The model developed by Ursino et al. represented this gas exchange process using mass-flow balance equations that incorporate outputs from the lung mechanics, pulmonary circulation, and blood-gas concentrations from the venous system, removing waste and reoxygenating the blood(Albanese et al., 2016). Simulink modeling started with the dead space gas fraction equations ($F_{D,\,O2,}$ and $F_{D,\,CO2}$) (Figure 2.8, labels 2 and 3), which determine the amount of oxygen and carbon dioxide inhaled and exhaled from the system while a Heaviside step-function dictates its period (Figure 2.8, label 1). Positive airflow ($\dot{V}$) acts as the inhalation period, drawing newly inspired air into the dead space, and negative airflow ($-\dot{V}$) acts as the exhalation and gas exchange period within the alveolar sacs. The programmed blood-gas disassociation equations ($C_{pp,\,gas}$) represent the amount of carbon dioxide and oxygen that can be removed or affixed for a given blood volume (V_{pp}) within the gas exchange period (Figure 2.8, label 7). The results of the blood-gas dissociation($C_{pp,\,gas}$), dead space gas fractions ($F_{D,\,O2}$ and $F_{D,\,CO2}$), pulmonary hemodynamics (Q_{pa} and V_{pp}), and deoxygenated venous blood-gas concentrations are input into the alveolar sac gas fraction equations ($F_{A,\,O2}$ and $F_{A,\,CO2}$) (Figure 2.8, label 4 and 5) which define the mechanics of removing and affixing gasses to the blood. The alveolar gas fractions ($F_{A,\,O2}$ and $F_{A,\,CO2}$) determine the total blood-gas concentrations of oxygen and carbon dioxide within the arteries ($C_{a,\,O2}$ and $C_{a,\,CO2}$) (Figure 2.8, label 8 and 9), the partial gas pressures (tensions) ($P_{a,\,O2}$ and $P_{a,\,CO2}$) (Figure 2.8, label 6), and the saturation of O_2 ($S_{a,\,O2} = S_{p,\,O2}$) (Figure 2.8, label 10) in the arterial blood transported to the left heart via the pulmonary vein (Q_{pv}) and later delayed.

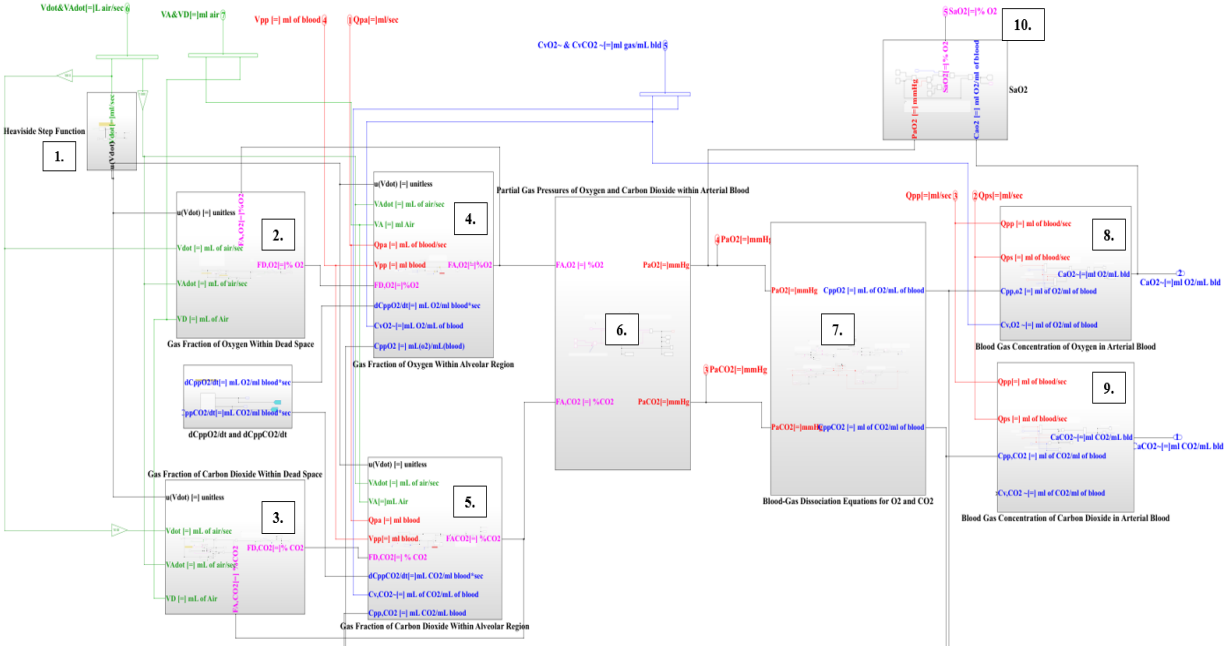

Figure 2.8: Lung Gas Exchange

2.3.10. Autonomic Nervous System Regulation

The autonomic nervous system (ANS) electrically regulates targeted regions of the body within a negative feedback control loop originating from receptors that transmit information to the CNS for processing and control via the sympathetic and parasympathetic systems of the ANS. Ursino et al. developed multiple iterations of a mathematical ANS model with a structure consisting of a sensory receptor region, sympathetic and parasympathetic ANS regulation, and regulated states connected in a negative feedback loop(Magosso & Ursino, 2001; Ursino, 1998; Ursino & Magosso, 2000). When modeling the ANS system, the goal was to combine different models to represent a negative feedback regulation system with the greatest number of sensors, effector signals, and regulated states to better represent the physiology of the autonomic system. The sensor region consists of equations approximating the afferent input signal response of the following: 1) peripheral chemoreceptors (f_{apc}) monitoring arterial blood-gas concentrations and pressures ($C_{a,\,gas}$ and $P_{a,\,gas}$) (Figure 2.9, label 1); 2) pulmonary lung stretch receptors (f_{ap})

monitoring lung tidal volume (V_{L_T}) (Figure 2.9, label 2); and 3) carotid baroreceptors (f_{ab}) monitoring systemic arterial pressure (P_{sa}) (Figure 2.9, label 3). Afferent signals connect with the sympathetic (Figure 2.9, label 5), parasympathetic (Figure 2.9, label 6), and respiratory (Figure 2.9, label 4) efferent control centers made up of phenomenological equations that summate the total sensory stimulation to determine the amplitude and frequency of response, determine the CNS response to hypoxia and offset the sympathetic signals, and directly connect with their regulated states. The excitatory sympathetic regulatory signals include 1) stimulation of the peripheral arterial vessel dilation/constriction (f_{sp}) (Figure 2.9, labels 7 to 9), 2) the initial unstressed volume of veins (f_{sv}) (Figure 2.9, labels 10 to 12), and 3) the contractility and pacing of the heart (f_{sh}) (Figure 2.9, labels 13 to 16) which additionally receives an inhibiting signal from the parasympathetic system (Figure 2.9, label 15). Finally, respiratory control regulates the depth of lung muscle activity (P_{mus}) and its rate of contraction (RR) based on chemoreceptors within the arteries (f_{apc}) (Figure 2.9, label 4).

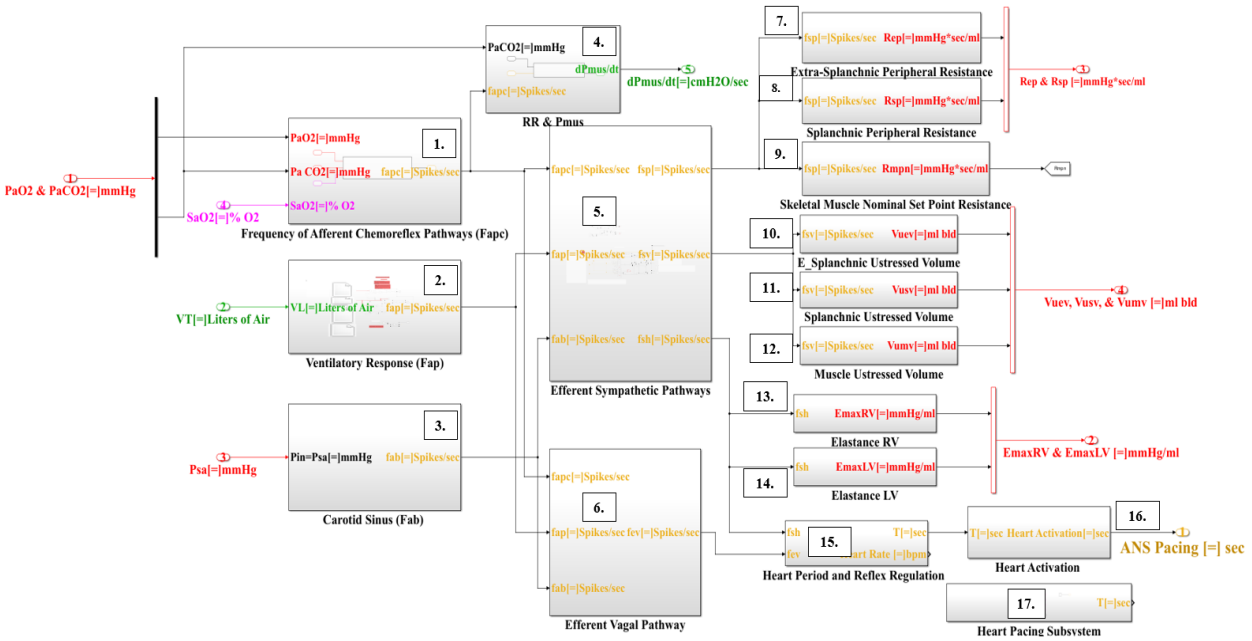

Figure 2.9: Autonomic Nervous System

2.3.11. Equation Testing and System Integration Process

Integrating multiple systems of equations into a single unified cardiopulmonary model involved first testing equations in isolation and then undergoing an iterative process of correlating and connecting system inputs/outputs, fixing critical compiler errors, resolving integration/differentiation issues, breaking algebraic loop instruction hazards, and modifying the model startup and initial conditions to improve stability. Testing system equations after modeling in Simulink involved applying test signal(s) as a simulated physiological waveform, resolving critical errors, and observing the output signals to find issues that could create integration problems for the final model. After initial testing, each system was brought into a single Simulink model, and the inputs and outputs of each system were connected. Integration involved an iterative process of correlating differing nomenclature used by Ursino et al. (i.e., Q and F meaning blood flow), connecting signals, mapping equation/system feedback loops, identifying missing connections or equation errors, and finding locations that created instability. The Simulink compiler computed the code and equations of the cardiopulmonary model under continuous-time conditions on a timestep interval that varied in length depending on maximum and minimum step size, error tolerance, and the ode23t trapezoidal method solver that could create compilation errors or instability in equations of the model. The linked ODE systems of the combined cardiopulmonary model were susceptible to integration and differentiation errors, where computing the solutions to equations with the compiler could create a hazard condition due to the step amount creating an infinite point, the signal input into a system equaling its natural pole, creating a divide by zero state, or an input creates unbounded increases/decreases in the system leading to instability. Both compilation and integration/differentiation errors required continuously tuning the compiler step and tolerance settings to avoid computational errors and

minimize simulation time, modifying initial conditions on different parts of ODEs, finding broken connections in the code equations, or buffering data to improve stability. The combined cardiopulmonary model's linked equations and parallel operations often created algebraic loops that would terminate simulations. Fixing these read-after-write memory hazards required identifying locations within the feedback loop of code that needed to be written to memory and buffering those operations to allow for parallelization in the model(MathWorks, 2023).

3. VERIFICATION OF THE COMBINED CARDIOPULMONARY MODEL

3.1. Verification Methods

Verifying the combined Simulink cardiopulmonary model involved assessing the accuracy of model-generated waveforms compared to the published results for the heart, systemic and pulmonary circulation, and lung mechanics systems seen in the published works of Ursino. This was accomplished by extracting data points from images of multiple published figures representing the steady-state function for a given system, extracting the respective waveforms generated by the Simulink model, interpolating the original Ursino data points to the length of the Simulink dataset, and then determining the mean squared error (MSE) and linear regression or R^2 value of the two datasets lined up in phase with one another. The accuracy of the Simulink model was determined by its R^2 value when comparing its data relative to the interpolated Ursino dataset. The standard of accuracy for a given system in the Simulink model was based on achieving an R^2 value of 0.85 or greater for its relation to the original Ursino model waveform and a mean squared error as close as possible to zero (Albanese et al., 2016; Magosso & Ursino, 2001; Ursino, 1998; Ursino & Magosso, 2000, 2002). This process was done to verify the function of the hemodynamic and lung mechanics system using as many available waveform diagrams as possible to evaluate the accuracy of the Simulink cardiopulmonary model. Model parameters (Appendix Table 1) and equations were set to match waveforms published by Ursino, which represent a healthy adult human male (Albanese et al., 2016; Magosso & Ursino, 2001; Ursino, 1998; Ursino & Magosso, 2000, 2002). A design consideration in developing the Simulink model was keeping the lung mechanics independent of the ANS system by assuming a constant amplitude and respiratory period rather than using the respiratory control mechanism outlined in the Albanese et al. paper. Each of the following

sections will outline the capability of the Simulink model to recreate the healthy normal systemic function seen in the various works of Ursino.

3.2. Verification of the Combined Cardiopulmonary Model

3.2.1. The Heart

Hemodynamic function within the left and right sides of the heart was assessed by analyzing the single-beat pressure-volume characteristic (Fig 3.1) and ejected blood flow out of the right and left ventricles (Fig 3.2), as well as the mechanical effect of the lungs on cardiac performance (Figure 3.3). Left ventricular pressure and volume were analyzed over a 0.95-second interval during normal steady-state conditions and with a constant respiratory period, to assess left ventricular systolic and diastolic function and its effect on systemic arterial pressure within the aortic arch (AoP) (Albanese et al., 2016; Ursino, 1998). The left ventricular waveforms were chosen at the apex of inhalation, where the hemodynamic amplitude was at its highest point. LVP, LVV, and AoP waveforms generated by the Simulink model achieved a high correlative value with the published data points with an $R^2>0.9$, while MSE was highest in LVP and LVV due to small differences in the filling and ejection curves (Figure 3.1).

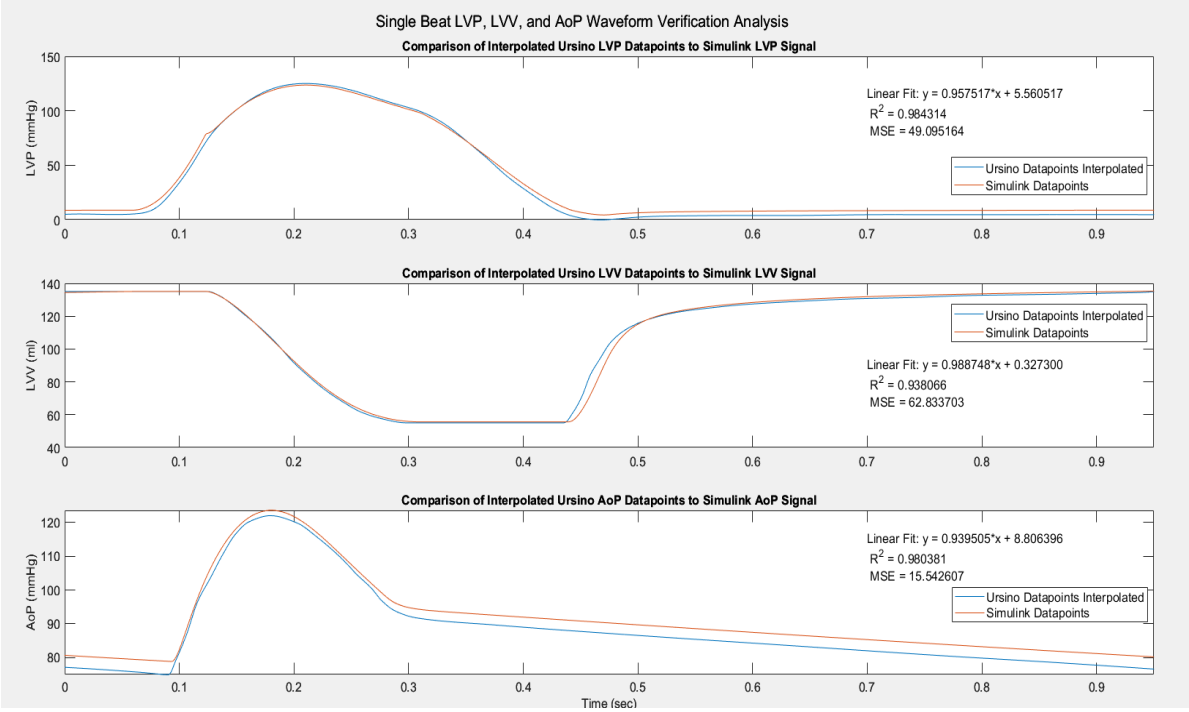

Figure 3.1: Left Ventricular Pressure, Volume, and Aortic Pressure Waveform Analysis of Extracted Data from Ursino (Albanese et al., 2016) compared to Simulink Waveform Data

Left and right ventricular outflow (F_{ol} and F_{or}, respectively) were examined over a 0.8-second interval to determine the function of the Simulink model's aortic and pulmonary valves relative to the results in the published waveforms (Albanese et al., 2016). F_{ol} and F_{or} correlated well with the Ursino data, with an R^2 value of 0.98 and 0.99, while the error between the two sets of waveforms was highest in F_{ol} due to the slight phase delay compared to the in-phase F_{or} waveform (Figure 3.2).

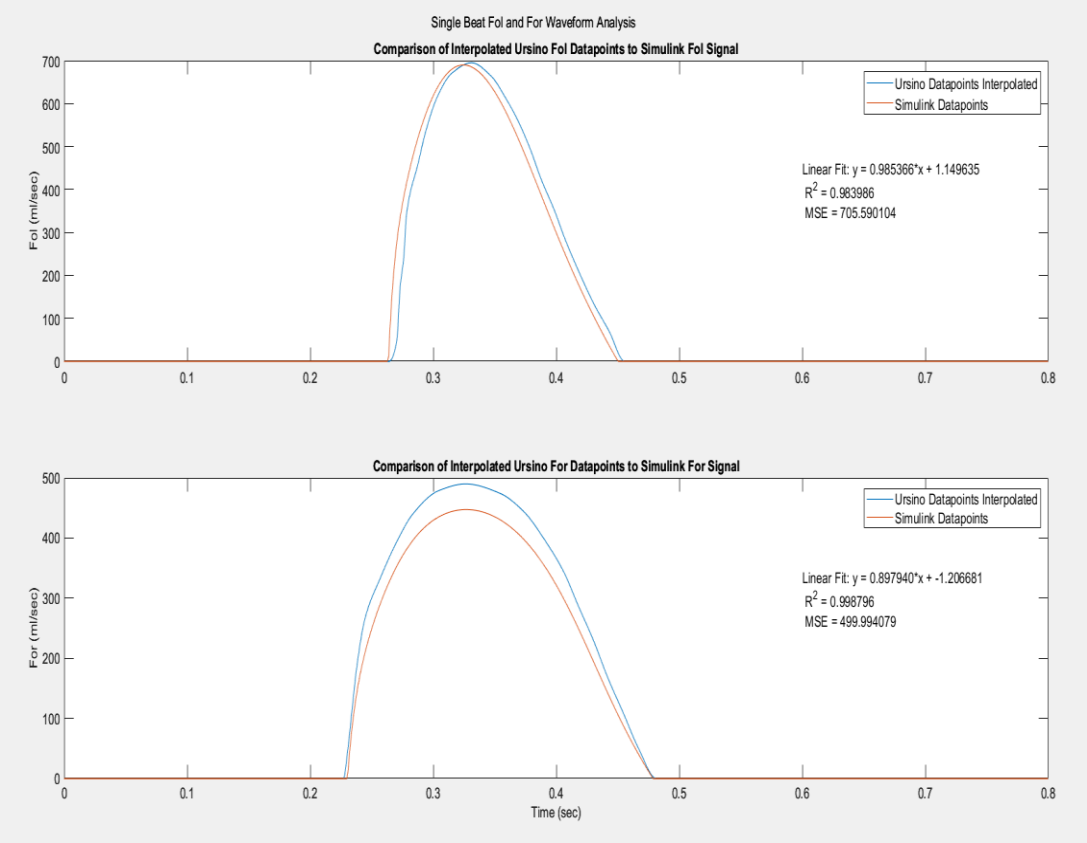

Figure 3.2: Left Ventricular (F_{ol}) and Right Ventricular (F_{or}) Outflow Waveform analysis of Extracted Data from Ursino (Albanese et al., 2016) compared to Simulink Waveform Data

The mechanical effect of the plural cavity pressure (P_{pl}) on venous return (VR) and right and left ventricular outflow (F_{or} and F_{ol}, respectively) and stroke volume (SV_r and SV_l, respectively) were studied over a twenty-second interval to verify the effect of respiration on cardiac input and output within the Simulink model (Albanese et al., 2016). Right and left ventricular outflows (F_{or} and F_{ol}) as well as right ventricular stroke volume (SV_r) were well correlated with the original Ursino data with an R^2 score of 0.87 with relatively low mean squared errors (Figure 3.3). Left ventricular stroke volume (SV_l) had a lower R^2 score of 0.69 and higher error with the original data due to the effect of respiration applied to the heart, which was outlined in the original model as a lower value due to the testing of the cardiac and respiration systems in isolation(Albanese et al., 2016). Venous return (VR) was out of phase

relative to the original model waveform and produced the lowest correlation and the highest error due to the interlinked effect of respiration applied on the return of blood to the right atrium, increasing the level of hemodynamic variation and lowing the amplitude.

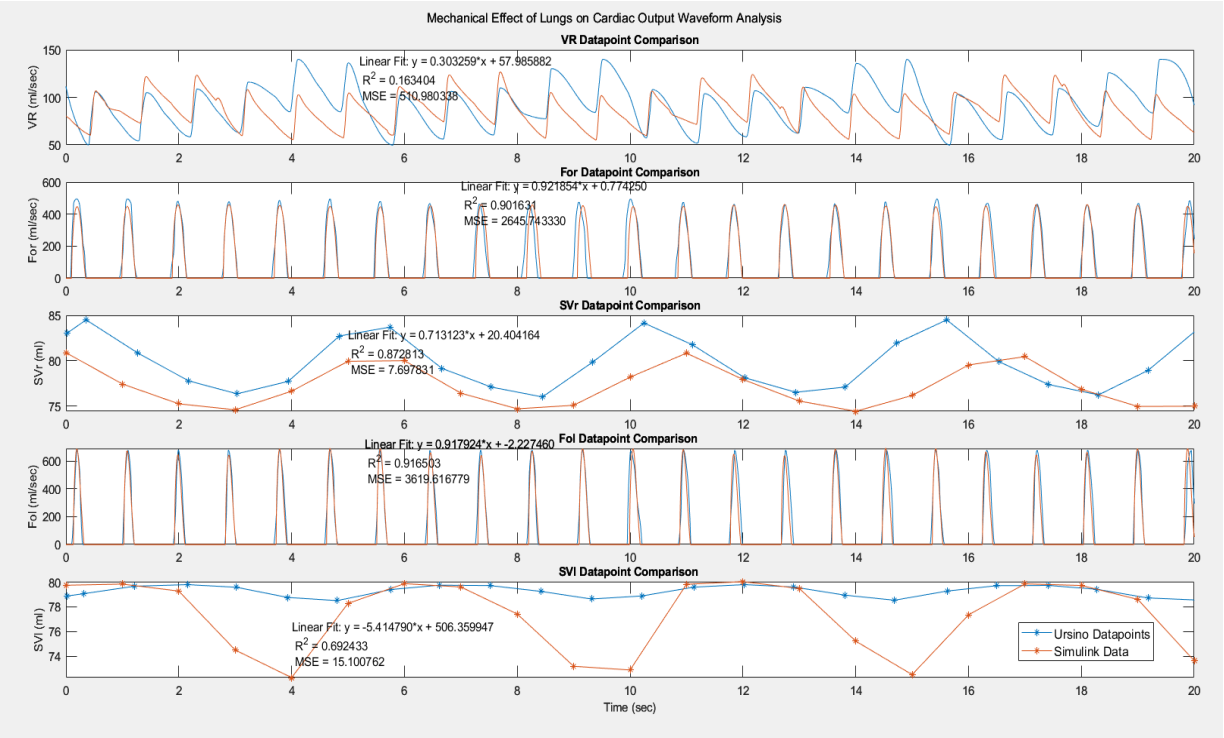

Figure 3.3: Mechanical Effect on Cardiovascular Performance adapted from Albanese et al., 2016 versus the Simulink Cardiopulmonary Model

3.2.2. Systemic and Pulmonary Circulation

Verifying the systemic and pulmonary circulation systems within the Simulink model involved studying mechanical respiration's effect on the systemic arteries' hemodynamics and determining blood pressure ranges throughout various cardiovascular regions. The interplay between systemic circulatory hemodynamics and the pleural cavity pressure (P_{pl}) from the lung mechanics system was studied over a 15-second interval. Pressure within the aortic arch (AoP is equivalent to P_{sa}) was recorded along with the beat-per-beat variance of systolic and diastolic blood pressure (SBP and DBP, respectively) within the systemic arteries under steady-state conditions and compared to the data points extracted from the publication waveforms (Fig 3.4)

(Albanese et al., 2016). Systemic arterial blood pressure correlated well with the original model waveforms with an R^2 score of 0.87 and MSE of 22 (Figure 3.4). Pleural Pressure (P_{pl}) did not correlate as directly to the original data due to the connection of the lung mechanics to the hemodynamics of the model and the independence of the respiration and hemodynamic systems introducing a phase delay. Systolic and diastolic blood pressure (SBP and DBP, respectively) had a decent correlation to the original data and a low MSE, that deviated due to the integrated effect of the lungs on the Simulink model's hemodynamics vs the isolated tests done on the original Ursino model (Albanese et al., 2016).

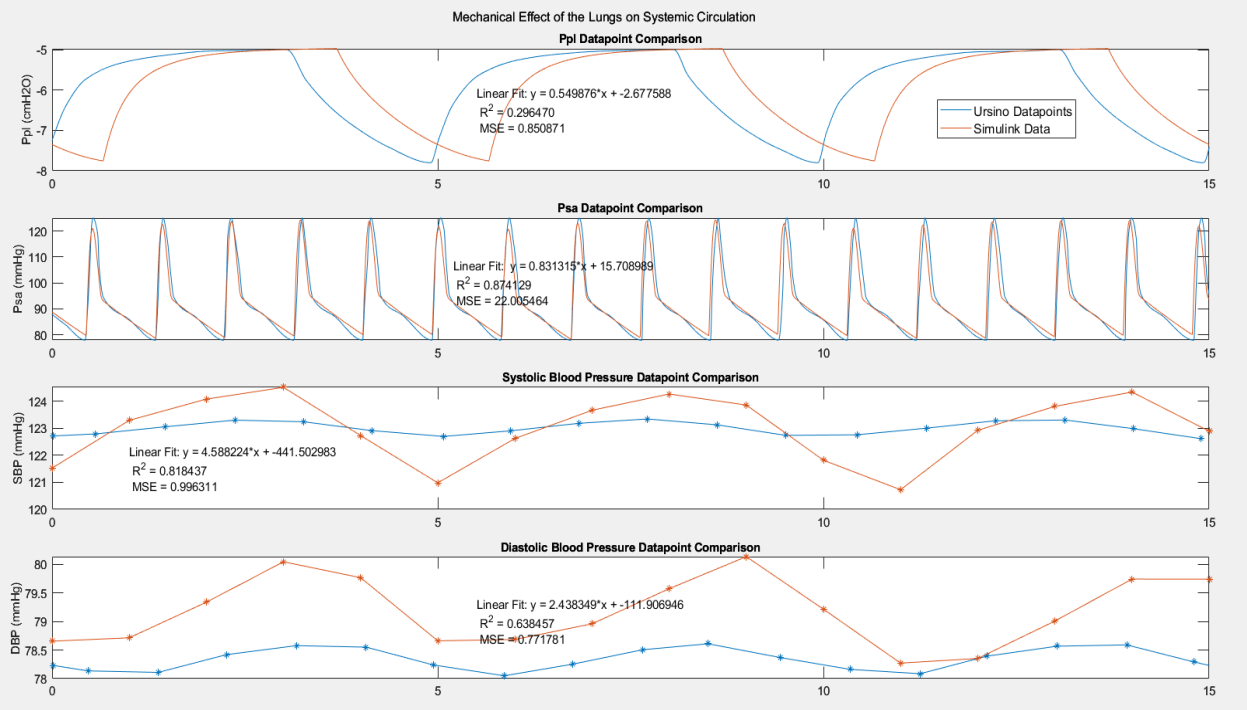

Figure 3.4: Pleural Pressure (P_{pl}), Aortic Pressure (P_{sa}), and Systolic and Diastolic Blood Pressure (SBP and DBP, respectively) Waveform analysis of Extracted Data from Ursino (Albanese et al., 2016) compared to Simulink Waveform Data

Pressure throughout the systemic, pulmonary, and heart regions of the Simulink model was verified by determining the systolic, diastolic, and average of the systemic arteries (P_{sa}), vena cava, right atrium, right ventricle, pulmonary artery, left atrium, and left ventricle and

comparing them to their standard ranges and the published results from the original model (Table 3.1) (Albanese et al., 2016). The hemodynamic blood pressure ranges generally matched well with normal systolic and diastolic pressure ranges published in medical literature and the original Ursino model(Albanese et al., 2016; Heldt et al., 2002; Lifesciences, 2022). Simulink model results trended towards the upper limits of pressure ranges in literature and deviated from the original published model in vena caval, right atrial, right ventricular, left atrial, and end-diastolic and systolic left ventricular pressures, more closely matching the literature ranges than Ursino's model.

Table 3.1: Comparison of Pressure Ranges for Healthy Patient Standard, Albanese et al. model, and the Simulink Cardiopulmonary Model

Pressure Variable [=] mmHg	**Standard Healthy Patient Pressure Ranges**	**Ursino Model Simulation Result (Albanese et al., 2016)**	**Simulink Cardiopulmonary Model Result**
Arterial Pressure (BP)	Systolic (SBP): 90-140 (Heldt et al., 2002)	Systolic (SBP): 122.79	Systolic (SBP): 120-124.5
	Diastolic (DBP): 60-90 (Heldt et al., 2002)	Diastolic (DBP): 78.86	Diastolic (DBP): 76.8-80
Mean Arterial Pressure (MAP)	70-105 (Lifesciences, 2022)	90.74	91.05
Vena Caval Pressure	Systolic: 2-14 (Heldt et al., 2002)	Systolic: 3.79	Systolic: 8.5
	Diastolic: 0-8 (Heldt et al., 2002)	Diastolic: 2.72	Diastolic: 7.07
Right Atrial Pressure (RAP)	2-6 (Lifesciences, 2022)	0.7	4.24-6.38
Right Ventricular Pressure (RVP)	Systolic: 15-28 (Heldt et al., 2002)	Systolic: 24.45	Systolic: 28.1-26.39
	Diastolic: 0-8 (Heldt et al., 2002)	Diastolic: -1.2	Diastolic: 2.61-4.8
Pulmonary Artery Pressure (PAP)	Systolic: 15-28 (Heldt et al., 2002)	Systolic: 24.41	Systolic: 26.4-28.19
	Diastolic: 5-16 (Heldt et al., 2002)	Diastolic: 7.38	Diastolic: 11.5-13.4
Left Atrial Pressure (LAP)	6-12 (Lifesciences, 2022)	4	6.11-9.3
Left ventricular Pressure (LVP)	Systolic: 90-140 (Heldt et al., 2002)	Systolic: 122.79	Systolic: 120-124.5
	End-Diastolic:4-12 (Heldt et al., 2002)	End-Diastolic: 0.2	End-Diastolic: 7.42- 8.46

3.2.3. Lung Mechanics

The mechanical function of the lungs within the Simulink model was verified under a steady rate of inhalation and exhalation to determine the amplitude and frequency of multiple regions versus the published model waveforms (Figure 3.5). The steady-state lung mechanical response of the respiratory muscles (P_{mus}), pleural cavity (P_{pl}), alveolar sacs (P_A), total airflow($\dot{V}$), lung volume (V_L), and the volume of the dead space were studied under a 15-second interval where the period of inhalation and exhalation was held at 5 seconds (Figure 3.5) (Albanese et al., 2016). After analyzing each of the regional pressures, total airflow, and regional volumes, the level of correlation with the original Ursino data was exceptionally high at an R^2 score ≥ 0.98 with an exceptionally low mean squared error for each waveform. The Simulink model lung mechanics system was accurately recreated as an independently driven system that interacts with the hemodynamics of the cardiovascular system (Figure 3.5).

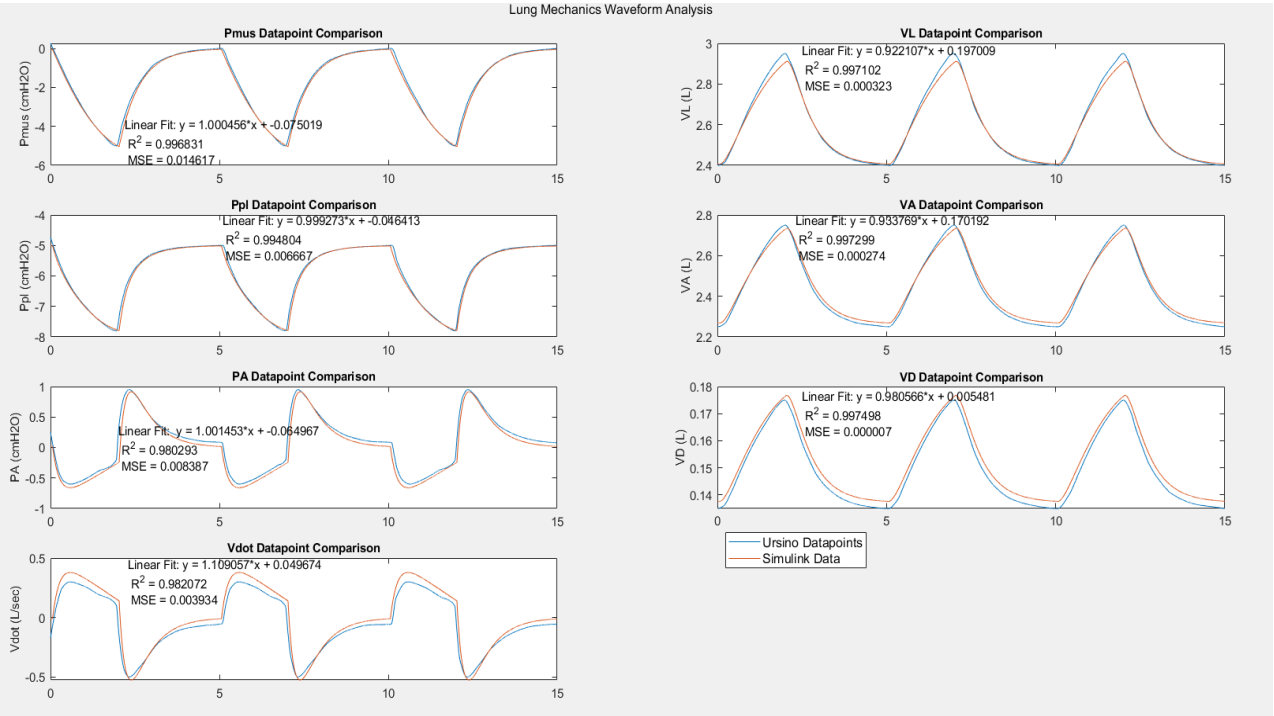

Figure 3.5: Air pressure, volume, and flow Lung Mechanics Waveform analysis of Extracted Data from Ursino (Albanese et al., 2016) compared to Simulink Waveform Data

4. VALIDATION OF THE INTEGRATED CARDIOPULMONARY MODEL

4.1. Introduction

After verifying the cardiovascular and lung mechanics systems within the combined cardiopulmonary Simulink model, its broader utility in research was validated by recreating an invasive pressure-volume (PV) loop study of the effects of vascular aging on cardiac performance. Modifying the base Simulink model parameters and system equations was required to adapt the system to simulate a PV loop study. Hemodynamic equations and their parameters within the left side of the heart, systemic circulation, and neurological control were tuned to achieve standard physiologic cardiac PV responses seen in the work of C. J. Wiggers and modern literature(Mitchell & Wang, 2014; Wiggers, 1923). A beat-per-beat processing algorithm was written in MATLAB to recreate beat summary data seen in literature and capture segmented instantaneous pressure-volume data points for the left ventricle for PV loop analysis. After model modification and tuning, additional modification to the code was done to simulate an autonomic nervous system blockade, right atrial pacing, constant respiratory rate, and a decrease in preload that mimicked an occlusion of the vena cava (VCO). Multiple sets of experiments were performed, first recreating the results of the Kelly study, then linearly varying compliance to observe the progression of vascular aging, and finally studying the frequency of pacing and its effects on normal and stiff compliance settings during steady state. These experiments validated the model's linearity and displayed its capability to recreate the cardiac trends and values for ventricular and vascular function and myocardial performance for vascular stiffening and for the force-frequency effect of the heart(Barodka et al., 2011; Endoh, 2004; R. P. Kelly et al., 1992; Redheuil et al., 2010).

4.2. Modifications to the Combined Simulink Cardiopulmonary Model

After verification of the base Simulink cardiopulmonary model, additional modification and tuning to the code was required to adapt it for use in simulating invasive cardiovascular studies. The primary target of this modification was to generate the physiologic cardiac responses seen in cardiovascular studies of healthy subjects (Mitchell & Wang, 2014; Wiggers, 1923). Model modification started with removing the CNS response to hypoxia within the chemoreceptor feedback loop and sympathetic and parasympathetic offset terms (θ_s and θ_v) to increase the sensitivity of the autonomic response to receptor inputs. Next, a parameter tuning process was performed on the sympathetic and parasympathetic weights of the ANS system ($W_{j,\,sp}$, $W_{j,\,sv}$, $W_{j,\,sh}$, and $W_{j,\,v}$) to increase autonomic tone and frequency, shifting the response of regulated states, such as peripheral arterial resistances (R_{ep}, R_{sp}, and $R_{mp,n}$), unstressed venous volumes (V_{uev}, V_{usv}, and V_{umv}), cardiac contractility ($E_{max,\,lv}$ and $E_{max,\,rv}$), and heart pacing (T). Hemodynamic parameters within the systemic circulation and autoregulation gain terms were tuned to bring aortic and parallel arterial pressures (AoP and $P_{arterial}$, respectively) within normal hemodynamic ranges(Mitchell & Wang, 2014; Wiggers, 1923).

Significant modifications to the original Simulink model equations were made to the left ventricle and the heart's activation function to adapt the system for use in a PV study of cardiac performance. The original left ventricular pressure and valve equations designed by Ursino were an exponential approximation of isometric left ventricular pressure based on the work of Sagawa et al. When tested under steady-state conditions, the pressure-volume data produced by the Ursino left ventricle model diminished amplitudes in LVP, dP/dt, and systemic arterial pulse pressure (PP) which were further exasperated when simulating the model under varying preload conditions, which showed insufficient results in our native condition model for left ventricular

stroke work (SW), pressure-volume area (PVA), and in measures of left ventricular contractility such as the end-systolic pressure-volume relationship (ESPVR), dP/dt_{max}-EDV, and preload recruitable stroke work (PRSW). The original left ventricle model isometric pressure ($P_{max,\,lv}$) was adapted to produce a nonlinear time-varying elastance element ($\varepsilon(t)$) that mimicked the behavior of cardiac tissue (Equation 1) (Drzewiecki et al., 1998; Ewert et al., 2004; Glantz, 1974; Glantz, 1975; Linke & Fernandez, 2002). The left ventricular pressure equation was modeled as an isometric pressure generated by the ventricle (HMP(t)) that decays because of the elastic and shortening losses of the myocardium (Equation 2)(Ewert et al., 2004; Suga, 1969, 1970). Left ventricular parameters were tuned to reproduce normal systolic and diastolic pressure ranges under steady-state conditions and achieve normal PV responses seen in healthy individuals, focusing on the issues with amplitude of LVP, LVV, and dP/dt, then on SW, PVA, ESPVR, dP/dt_{max}-EDV, and PRSW during varied preload conditions (Figure 4.1). The final area of modification was Ursino et al.'s activation function of the heart, which represents the duration of contraction (systole) and relaxation (diastole) (Ursino, 1998). As heart rate increased during pacing, the hemodynamic and contractile behavior exponentially decreased due to the design of Ursino's original activation function linearly increasing the duration of systole without limit, displaying a reduced cardiac contractility and significantly reduced cardiac output, running contrary to literature(Ricci et al., 1979; Schaefer et al., 1988). This issue was remedied by designing a nonlinear curve fit function (Equation 3) to determine the duration of systole (T_{sys}) and scale it proportional to diastole to allow for increased filling time and display the PV response seen in high heart rates (Ricci et al., 1979; Schaefer et al., 1988).

$$\varepsilon(t) = \frac{P_{max,lv}(t)}{V_{lv}(t)} = \frac{\varphi(t)\cdot E_{max,lv}(t)\cdot\left(V_{lv}(t)-V_{u,lv}\right)+[1-\varphi(t)]\cdot P_{0,lv}\cdot\left(e^{k_{E,lv}\cdot V_{lv}(t)}-1\right)}{V_{lv}(t)} \quad \text{(Eq.1)}$$

$$LVP(t) = HMP(t) - \Delta P_{elast} + k_{R,lv}\cdot P_{elast}(t)\cdot\frac{dLVV}{dt} \quad \text{(Eq.2a)}$$

$$LVP(t) = \varepsilon(t) \cdot \left[EDV - V_o - V_{eject}\right] + k_{R,lv} \cdot P_{elast}(t) \cdot (F_{il} - F_{ol}) \quad \text{(Eq. 2b)}$$

$$T_{sys} = -T_{sampled}{}^2\left(HR_{sampled} - 60\right) - (0.4249)T_{sampled}{}^2 + T_{sampled} \cdot T_{sys0} \quad \text{(Eq.3)}$$

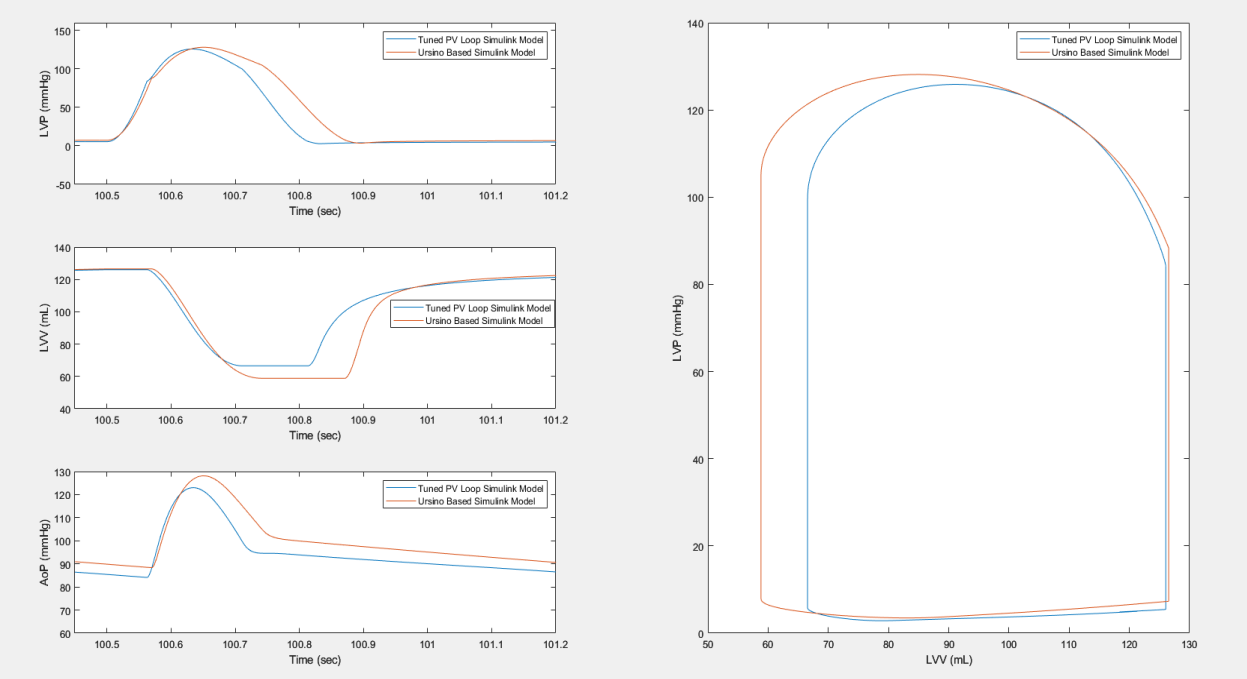

Figure 4.1: Comparison of Cardiac Response of Tuned Simulink PV Model (Blue) vs Ursino Parameter Simulink Model (Red)

4.3. Validation Methods

The hemodynamics of the Simulink cardiopulmonary model were validated by recreating the experimental setup and procedure of an invasive PV loop study done by Kelly et al. using multiple canine subjects and observing the effects of aortic stiffening on ventricular-vascular function and cardiac performance(Raymond P Kelly et al., 1992). Ten autonomically blocked canine subjects who each had undergone a grafting of a stiff plastic conduit on their descending aorta, had their vena cava occluded while blood flow out of the heart was directed via an aortic clamp through the native condition ascending aorta or the stiff Tygon tubing(Raymond P Kelly et al., 1992). Arterial models were derived for the native and stiff compliance using the left

ventricular PV data recorded during the steady-state and occluded periods. The study gave insights into the effect of a stiffening vasculature on the function of a healthy heart and a projection for the myocardial performance for human patients (Raymond P Kelly et al., 1992).

To recreate the experimental setup of the Kelly experiment using the Simulink model, the organization of the systemic arterial compartments was changed, and additional code was developed within Simulink and MATLAB to recreate an autonomic beta-blockade, hold respiration constant, pace the heart, and simulate a vena caval occlusion (VCO). The following sections will outline the experimental design and summarize the results and impact; further details and results can be found in the articles published and cited with this thesis work(Mulligan, Mitrev, et al., 2024; Mulligan et al., 2023; Mulligan, Ungerleider, et al., 2024).

4.3.1. Organization of the Arterial System into Proximal and Distal Elements

The arterial system structure of the Simulink model was organized into a proximal and distal arterial region that forms a combined Windkessel model (Figure 4.1). Blood flows out of the left ventricle (F_{ol}) and enters the aortic arch region (Figure 4.1 label 1 to 2), that defines the mechanics of the proximal segment of the systemic arteries. Flow to the systemic arteries (F_{sa}) then connects in series with the distal region of the vascular Windkessel model (Figure 4.1 label 3 to 4), which consists of a mass-flow balance differential equation that determines the parallel pressure of the five regions (Figure 4.2).

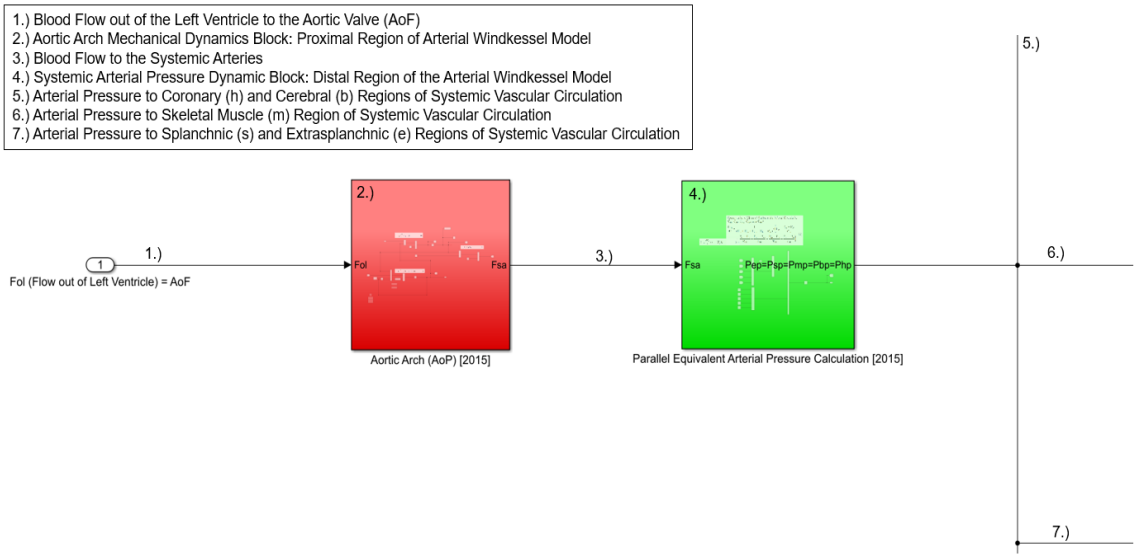

Figure 4.2: Overview of Simulink CM's Proximal and Distal Arterial Elements

Inflow from the aortic arch is divided into the five parallel branches of the vascular system (Fig 4.2 label 1 to 2), each of whom consists of its constant compliance element that combines to form the equivalent compliance of the arterial system ($C_{p,\ equivalent}$) (Fig 4.2 label 3). Arterial load within this distal region varies depending on autonomic stimulation and local-effect autoregulation of hemodynamic resistance, varying the total blood flow of each region. The proximal and distal regions of the vascular system combine in series, dictating the hemodynamics within the systemic circulation of the Simulink model (Fig 4.1).

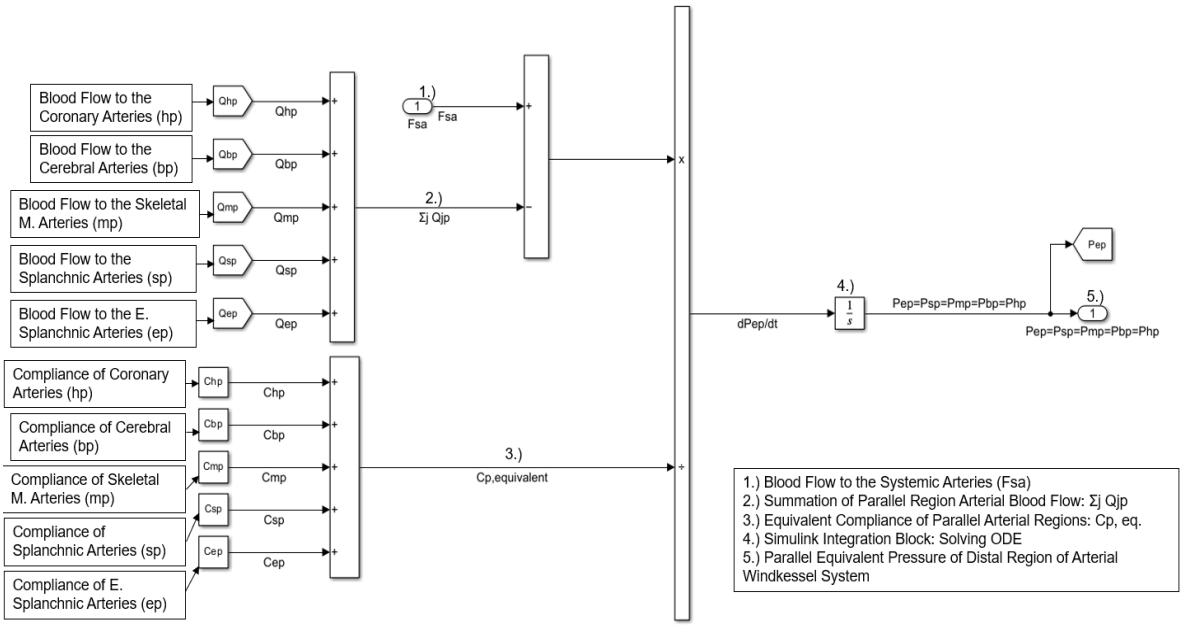

Figure 4.3: Simulink Cardiopulmonary Equivalent Hemodynamic Pressure Equation of the Distal Arterial Region

4.3.2. Experimental Model Design

Additional modification of the code was taken to recreate the procedure of Kelly et al. and in invasive PV loop studies using a blockade of the ANS system, right atrial pacing, and a VCO to decrease preload and stress the cardiac system(Raymond P Kelly et al., 1992). A MATLAB function was developed within Simulink that divides the signals from the ANS model into two parallel paths: a startup pathway that allows ANS regulation to bring the model to steady state and a blockade pathway that holds autonomic stimulation and respiratory rate constant for the period of the occlusion study. During a blockade, the values exiting the code are constant for fsp, fsv, fsh, and fev, keeping the regulated states at a constant value while the rate of respiration is held at zero, inducing a steady breathing rate that removes the influence of lung mechanics on cardiovascular performance. Right atrial pacing is simulated similarly to the ANS blockade by allowing the heart period (T) to vary until it reaches steady state and then holding it constant over the occlusion period (i.e., T = 1 for HR of 60 bpm). A vena caval occlusion was

simulated within the model using a step increase in hemodynamic resistance of the thoracic veins (Rtv), which pools the venous blood together from the five parallel vascular compartments and returns it to the right atrium (Q_{tv} is equivalent F_{ra}). Obstructing flow within this region mimics the effect of reducing preload to the heart, representing an obstruction of the inferior and superior vena cava. The Simulink model VCO simulation process involves 1) running the model to a steady state under unmodified conditions for 100 seconds within the simulation, 2) pacing the heart at a specified amount and enabling the ANS blockade for the remainder of the simulation, 3) at 199 seconds into the simulation, the step increase in thoracic vein resistance starts and lasts for a 10-second interval and releases. Data is captured in a beat-per-beat processing MATLAB algorithm that starts at one beat prior to the VCO to the apex of the occlusion period, recording standard hemodynamic summary measurements and segmented PV data points corresponding to each of the recorded beats.

4.3.3. Adapting the Kelly et al. Vascular System to the Simulink Model

Due to the vast differences in the cardiovascular structure between the canine subjects within the Kelly et al. study and the human Simulink model, an adaptation process was required to achieve comparable results and verify the nature of the experimental setup(Raymond P Kelly et al., 1992). Aortic arch compliance (C_A) and total peripheral resistance (R_T) for the native and stiff Tygon models were altered from their original study values while keeping the PV response consistent with the behavior and results seen in Kelly et al. (Figure 4.3) (Raymond P Kelly et al., 1992). Native model compliance and resistance were changed from a C_A = 1.65 ml/mmHg to C_A = 0.7 ml/mmHg (Figure 4.3 A), while the stiff Tygon compliance value of C_A = 0.19 ml/mmHg was used from the original study due to it simulating within the Simulink model and recreating the vascular aging effect(Figure 4.3 B). Total peripheral resistance was modified from the canine

normal R_T = 3.04 mm Hg* ml^{-1} * sec^{-1} to R_T = 1.28 mm Hg* ml^{-1} * sec^{-1} while the resistance of the stiff Tygon conduit was kept at the value of R_T = 3.66 mm Hg* ml^{-1} * sec^{-1}.

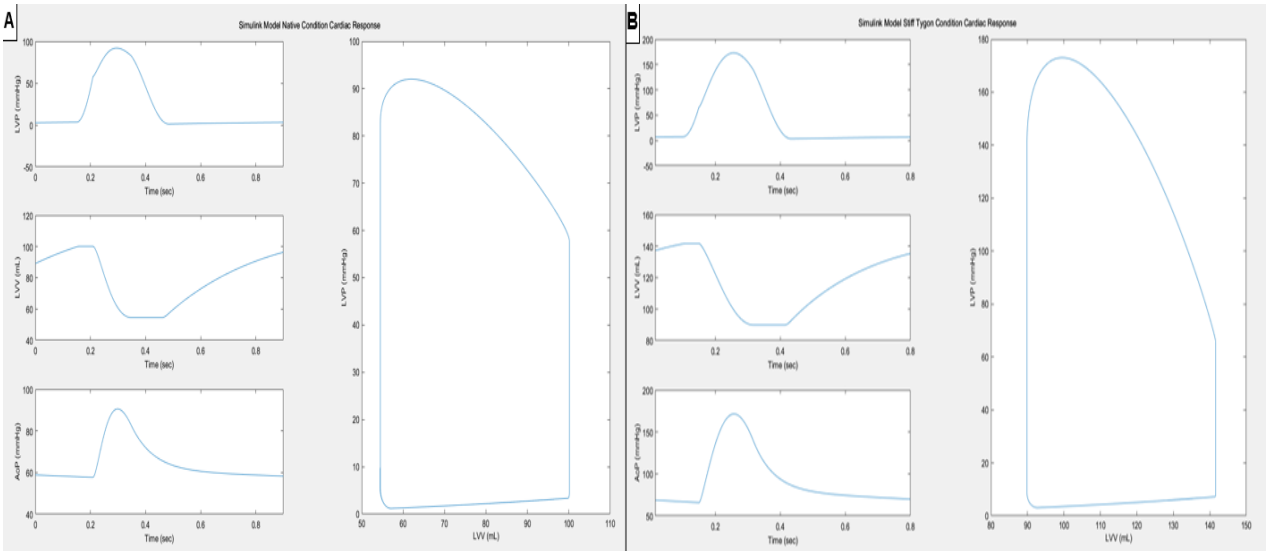

Figure 4.4: A single-beat snapshot of Pressure-Volume data in the adapted Native (A) and Tygon (B) models

4.3.4. Linear Modification of the Proximal Compliance Element (C_A)

After achieving results comparable to those of the native and Tygon models, compliance was linearly modified within the proximal aortic arch region (C_A) to determine the linearity of the Simulink model and gain further insights into cardiovascular function as vascular load changes. The heart was paced at 80 bpm, and vascular load was linearly modified by proportionally reducing compliance from native conditions (C_A = 0.7 ml/mm Hg and R_T = 1.28 mm Hg* ml-1 * sec-1) down to the Tygon compliance (C_A = 0.19 ml/mm Hg and R_T = 3.66 mm Hg* ml-1 * sec-1). Starting from native compliance, it was decreased by 10 percent to C_A = 0.63 ml/mm Hg and R_T = 1.41 mm Hg* ml-1 * sec-1; by 20 percent to a C_A = 0.56 ml/mm Hg and R_T = 1.54 mm Hg* ml-1 * sec-1; then down 40 percent to C_A = 0.42 ml/mm Hg and R_T = 1.805 mm Hg* ml-1 * sec-1; and finally to the Tygon compliance and resistance C_A = 0.19 ml/mm Hg and R_T = 3.66 mm Hg* ml-1 * sec-1.

At each compliance and resistance level, the impact of left ventricular and vascular coupling was studied using standard clinical indexes, such as left ventricular volume (EDV, ESV, and SV), end-systolic and end-diastolic pressure (Pes and EDP, respectively), pulse pressure (PP), SW, and dP/dtmax, that were each captured for every beat of the VCO along with segmented PV data for every corresponding beat. The pressure-volume data was used in a linear least-squares curve fit to derive measures of cardiac contractile function such as the end-systolic pressure-volume relation (ESPVR), the stroke work and EDV relation, dP/dtmax-EDV, pressure-volume area, and mechanical efficiency to understand the impact of aortic stiffening. Results were verified using prior research on cardiac contractile function and performance and the study by Kelly et al. (Freeman, 1990; R. P. Kelly et al., 1992; Kolh et al., 2000).

4.3.5. Heart Rate Modification on Native and Stiff Aortic Compliance Models

The increasing force produced by the heart by increasing heart rate (force-frequency effect) was studied using the Simulink model under normal and stiff compliance conditions during the steady-state beat before a vena caval occlusion (Barodka et al., 2011; Endoh, 2004). Compliance was maintained at native or stiff conditions while pacing the heart at 60, 100, and 140 beats per minute. Beat-per-beat summary data was recorded for the three frequencies and their PV data points to derive the same ventricular-vascular coupling and contractile performance metrics described in the prior section. The two sets of data were validated using research published by Kelly et al. and other literature describing the effects of vascular stiffening combined with heart rate on cardiac function and performance (Barodka et al., 2011; R. P. Kelly et al., 1992; Redheuil et al., 2010).

4.4. Results

4.4.1. Impact of Linear Decrease in Compliance (C_A) on Cardiovascular Dynamics

Linearly decreasing compliance of the aortic arch from its native to stiff setting increased the average beat-per-beat hemodynamic values for ventricular and vascular volume and pressure(Mulligan, Mitrev, et al., 2024). End diastolic and systolic volumes grew gradually as compliance decreased, while SV only slightly increased. End systolic pressure (Pes) grew significantly from 81.7 to 133.6 mmHg, while left ventricular end-diastolic pressure (LVEDP) only marginally grew from 5 to 8.4 mmHg. Stroke work (SW), pulse pressure (PP), and dP/dtmax significantly grew, matching the literature for increased vascular stiffness, starting at 3830 mmHg*ml, 33.4 mmHg, and 1621 mmHg/sec at normal and then growing to 7313 mmHg*ml, 106.6 mmHg, and 2057 mmHg/sec, respectively(Barodka et al., 2011; R. P. Kelly et al., 1992; Moulton & Secomb, 2023). Additionally, the estimated arterial compliance (C_a) decreased due to the significant increases in SW, PP, and Pes from native to stiff aortic compliance.

When examining the effect of reduced aortic compliance on cardiac contractility and efficiency, overall performance was reduced due to the increase in C_A's stiffness(Mulligan, Mitrev, et al., 2024). ESPVR gradually reduced, starting at normal at 1.8 and reducing to 1.57 at the stiff Tygon compliance. Mechanical efficiency (ME) was reduced over compliances, starting at 71.1 %, which was normal, and reducing to 60.5%. The reduced efficiency was further emphasized by a significant increase in preload-recruitable stroke work (PRSW) starting at 71.4 and going to 94.8 and in the EDV pressure-volume area (PVA) relation going from 91.7 to 154.7. There were no considerable changes for dP/dtmax-EDV.

4.4.2. Impact of Increasing Heart Rate on Cardiovascular Dynamics of the Native and Stiff Compliance

Varying the heart rate from 60, 100, and 140 bpm at the native and stiff settings reduced pressures and volumes as pacing increased with the baseline starting amplitudes changing depending on the compliance of the aortic arch (Mulligan, Mitrev, et al., 2024). Left ventricular volumes EDV and ESV reduced as heart rate increased, starting at an SV of 58.5 ml and dropping to 26.7 ml for native conditions, while the stiff conditions produced a similar result, beginning at 66.6 ml and dropping to 26.7 ml at 140 bpm. End systolic pressure (Pes) only slightly decreased from 82.8 to 72.1 mmHg under normal and had a more significant change under stiff conditions, dropping from 141.1 to 72.1 mmHg. Stroke work followed the same trend as Pes dropping significantly as heart rate increased starting at 5078 to 1923 mmHg*ml for normal and 10322 to 3989 mmHg*ml for stiff. EDP for the left ventricle under normal conditions remained relatively unchanged while it significantly grew under the Tygon compliance.

When examining the contractile state and efficiency results, the force-frequency relationship was demonstrated in the Simulink model for ESPVR and the dP/dtmax-EDV relationship, increasing gradually for normal and stiff compliances(Endoh, 2004). Measurements of cardiac efficiency such as PRSW, ME, and EDV-PVA demonstrated the same trend as the previous study, decreasing as compliance dropped and heart rate increased. Preload recruitable stroke work (PRSW) gradually decreased from 82.5 at 60 bpm to 56.5 at 140 bpm under native, while the drop in stiffness was significant, going from 118.5 to 54.6(Mulligan, Mitrev, et al., 2024). The change in mechanical efficiency (ME) slightly decreased for normal and stiff settings, with the starting point at 60 bpm 76.4% and 65.8%, respectively. EDV-PVA showed a

slight decrease from 100.6 to 79.1 for normal, while stiff showed the same trend, starting with a much greater area at 182.1 and dropping to 131.2.

4.5. Discussion of Validation Results

The Simulink model validation process proved that the original design of Ursino could be extended and developed into a research tool for the simulation of an invasive PV loop study, was capable of generating pressure-volume data that matched previous literature and recreating a research scenario that was not feasible for human subjects. Initial results of the study under the native and stiff Tygon compliance settings matched the general hemodynamic trends for ventricular and vascular function metrics and cardiac performance, with elevated hemodynamics and reduced efficiency as compliance dropped, as seen in the Kelly et al. study and literature (Barodka et al., 2011; R. P. Kelly et al., 1992; Redheuil et al., 2010).

After verifying the initial results of the model, the work of the original Kelly et al. study was furthered by investigating the effect of progressing vascular aging by linearly varying compliance and peripheral resistance. Linearly decreasing aortic arch compliance and increasing peripheral resistance from native to stiff conditions on multiple intervals displayed the progression of vascular aging and illustrated the gradual loss of cardiovascular performance and energetics as vascular load increases(Barodka et al., 2011; R. P. Kelly et al., 1992). From native to stiff conditions, ventricular and vascular function hemodynamic metrics such as SV and Pes significantly increased, resulting in higher stroke work and reduced cardiac mechanical efficiency, which worsened as compliance was reduced. As vascular aging progressed, the significant losses in efficiency and the increased work and PV area match the trends outlined in cardiovascular literature(Barodka et al., 2011; R. P. Kelly et al., 1992; Moulton & Secomb, 2023; Redheuil et al., 2010). The effect of increasing the simulated vascular aging demonstrates

the gradual or exponential changes in cardiovascular function that can contribute to or cause morbidity in patients, such as the increased stress on the heart through the increased energy and work demands leading to damage to the myocardium and possible future disease(Barodka et al., 2011; Raymond P Kelly et al., 1992). The series of experiments that were performed in this linear compliance modification study verified the linearity of the Simulink model and highlighted its capabilities as a research tool allowing the user to simulate precise modification of key cardiovascular parameters that could not be feasibly done in traditional invasive cardiac studies.

Studying the effect of increasing heart rate on high and low compliance settings demonstrated the impact of increasing heart rate on the force produced by the heart and began investigating the impact of reduced aortic compliance at increasing heart rates. The results demonstrated a significant loss in cardiac efficiency in increased PRSW and EDV-PVA, while mechanical efficiency was considerably reduced at high heart rates for the stiff Tygon condition model. The significant reductions in cardiac efficiency at high heart rates demonstrate the adverse effects of a high vascular load combined with tachycardia for patients and the health of their heart(Mitchell, 2008).

5. DISCUSSION AND CONCLUSION

5.1. Discussion

This work accomplished its goals of developing a unified cardiopulmonary model built upon the work of Ursino et al. within the Simulink and MATLAB development environment, the testing and verification of the hemodynamics and lung mechanics systems and beginning the further development of the integrated model into code that can accurately simulate an invasive pressure-volume study. Integration of the multiple models developed over multiple decades was an intensive process of testing, tuning, and refining the code to combine multiple systems into a cohesive system within the Simulink environment, which was facilitated by the multiple toolboxes and integration tools built within MATLAB to achieve a stable and functional model. The focus after integration was verifying the integrity of the hemodynamic and lung mechanics models due to the emphasis on applying the Simulink model for the simulation of an invasive PV loop study. Results from verification showed a good correlation between the extracted data points from published hemodynamic waveforms and lung mechanics, with differences arising due to the design decisions to keep the lung mechanics separate and differences in the approach taken in integrating equations and parameters in the Simulink model versus the approaches taken by Ursino et al. in their combined cardiopulmonary model(Albanese et al., 2016). The additional modification to cardiopulmonary parameters and equations for validation started iterating and furthering the work developing the Simulink model into a system capable of producing physiologic cardiac responses for use in a simulated PV loop study. Validation of the model using a simulated vena caval occlusion to study the effect of vascular aging and increased heart rate at normal and stiff compliance settings showed the capabilities of the Simulink cardiopulmonary model as a research tool. Results from the study recreated published results on

PV interactions, ventricular-vascular coupling, and the force-frequency effect and provided additional insights into the effects of how reduced compliance significantly reduces the performance of the myocardium (Mulligan, Mitrev, et al., 2024; Mulligan et al., 2023; Mulligan, Ungerleider, et al., 2024).

5.2. Limitations of the Simulink Cardiopulmonary Model

The approach taken by this work in developing the Simulink cardiopulmonary model involved using published lumped-parameter models of the cardiovascular system only partially integrated all systems described by Ursino et al. and did not fully verify every system described in the combined cardiopulmonary model Lumped-parameter models describe the global dynamics of a given system rather than the segmented and interlinked dynamics seen in Multiphysics or multiscale models. The advantage of designing the Simulink model using lumped parameter models was the capability to unite multiple dynamic systems together and get results instantaneously for the global performance of a system, compared to Multiphysics models of the cardiovascular system that provide a high degree of spatial and temporal information at the cost of high computational time. The Simulink model assumes that spatial components of the partial differential equations that define the hemodynamics of the cardiovascular system are constant and focus on the global instantaneous solution within the temporal domain. Additionally, the system equations focus on an electric analog or 3-element Windkessel system and do not include parameters or equations that allow for the study of pulse-wave velocity or reflections and their effects on vascular dynamics. Respiratory control within the Simulink model is a constant varying waveform that did not incorporate the dynamic control model outlined by Ursino due to limitations of the scope of this work and instabilities in integrating the system equations during the early phases of development(Albanese et al., 2016). This missing

element of respiratory control limits the Simulink model's use in future studies of respiratory disease or simulated exercise. Additionally, the lung-gas exchange, tissue-gas exchange, venous-pool gas transport, ANS regulation, and autoregulation subsystems have not yet been verified and will need further verification or development for future use of the model in other research areas.

5.3. Future Work

The original design focus of Ursino's system equations used in creating the Simulink model was primarily on respiratory dynamics and their effects on hemodynamics and control, with less emphasis on the dynamics of the cardiovascular system. This work started development into creating a PV loop model during the validation phase, but additional work is required to fix key issues with the cardiac dynamics. The model uses a Windkessel approach to representing the heart and neglects some key dynamics of the myocardium, the valves, and the impact of electrical and mechanical dynamics on the heart(Albanese et al., 2016; Ursino, 1998). This limits the use of the model for studying chronic heart failure or cardiac dyssynchrony and potential ways of mitigating it through therapy. Additionally, ESPVR and EDPVR are assumed to be linear at all heart volumes, which frequently made it unstable due to Ursino assuming the heart would only operate within healthy limits rather than lower or higher ventricular volumes. This instability was because this linear approach assumes that the heart model can contract without any limitation on its stretched length, neglecting the force-length limitations of the heart(Grodins, 1959; Starling, 1918; Wiggers, 1923).

Further research can focus on developing the Simulink model as a research tool and a digital twin of the human body. A major benefit of the MATLAB and Simulink environment is the scalability and integration tools that facilitate adding new system equations to the existing

model. Future work can focus on adding a dynamic metabolic system, additional ANS reflex pathways, temperature control, respiratory study and experimentation, hormone control, renal circulation and regulation, etc. The major goal of this thesis is to begin developing a platform for the future development of a digital twin of the human body that contains these key systems. Function within the human body is complex and built upon multiple dynamic interactions that combine to sustain life. Suppose we can begin adding and integrating these interactions. In that case, we can gain further insight into the effects of diseases and treatment or find new emergent insights into the function of the human body.

5.4. Conclusion

This Simulink model developed an integrated cardiopulmonary model focusing on hemodynamics and PV interactions within the heart and vascular system. The findings provide insight into the effects of vascular aging on the cardiovascular system, reduced compliance as morbidity, and its effect on high heart rates. A future goal is to continue the work toward developing this system into a digital twin of the human body.

REFERENCES

Albanese, A., Cheng, L., Ursino, M., & Chbat, N. W. (2016). An integrated mathematical model of the human cardiopulmonary system: model development. *American Journal of Physiology-Heart and Circulatory Physiology*, *310*(7), H899-H921. https://doi.org/10.1152/ajpheart.00230.2014

Asai, A., Konno, M., Taniguchi, M., Vecchione, A., & Ishii, H. (2021). Computational healthcare: Present and future perspectives (Review). *Exp Ther Med*, *22*(6), 1351. https://doi.org/10.3892/etm.2021.10786

Barodka, V. M., Joshi, B. L., Berkowitz, D. E., Hogue Jr, C. W., & Nyhan, D. (2011). Implications of vascular aging. *Anesthesia & Analgesia*, *112*(5), 1048-1060.

Danz, A. (2020). *getDataTips-Get data tip text and handles*. In (Version 1.0.1) https://www.mathworks.com/matlabcentral/fileexchange/82038-getdatatips-get-data-tip-text-and-handles

Drzewiecki, G. M., Li, J. K., Palladino, J. L., & Noordergraaf, A. (1998). Muscle contraction mechanics from ultrastructural dynamics. *Analysis and Assessment of Cardiovascular Function*, 33-57.

Endoh, M. (2004). Force–frequency relationship in intact mammalian ventricular myocardium: physiological and pathophysiological relevance. *European journal of pharmacology*, *500*(1-3), 73-86.

Ewert, D., Wheeler, B., Doetkott, C., Ionan, C., Pantalos, G., & Koenig, S. C. (2004). The Effect of Heart Rate, Preload, and Afterload on the Viscoelastic Properties of the Swine Myocardium. *Annals of Biomedical Engineering*, *32*(9), 1211-1222. https://doi.org/10.1114/b:abme.0000039355.53117.6f

Frank, O. (1899). des Arteriellen, F O Die Grundform Pulses. *Zeitschrift zur Biologie*, *37*, 483-526.

Frank, O. (1990). The basic shape of the arterial pulse. First treatise: mathematical analysis. *Journal of molecular and cellular cardiology*, *22*(3), 255-277.

Freeman, G. L. (1990). Effects of increased afterload on left ventricular function in closed-chest dogs. *Am J Physiol*, *259*(2 Pt 2), H619-625. https://doi.org/10.1152/ajpheart.1990.259.2.H619

Glantz, S. A. (1974). A constitutive equation for the passive properties of muscle. *Journal of biomechanics*, *7*(2), 137-145.

Glantz, S. A. (1975). A three-element model describes excised cat papillary muscle elasticity. *American Journal of Physiology-Legacy Content*, *228*(1), 284-294.

Grodins, F. S. (1959). Integrative Cardiovascular Physiology: A Mathematical Synthesis of Cardiac and Blood Vessel Hemodynamics. *The Quarterly Review of Biology*, *34*(2), 93-116. https://doi.org/10.1086/402631

Guyton, A. C., Coleman, T. G., & Granger, H. J. (1972). Circulation: overall regulation. *Annual review of physiology*, *34*(1), 13-44.

Heldt, T., Shim, E. B., Kamm, R. D., & Mark, R. G. (2002). Computational modeling of cardiovascular response to orthostatic stress. *Journal of applied physiology*, *92*(3), 1239-1254.

John, E. (2011). Guyton and Hall Textbook of Medical Physiology 12th Edition. In: Saunders.

Kelly, R. P., Tunin, R., & Kass, D. (1992). Effect of reduced aortic compliance on cardiac efficiency and contractile function of in situ canine left ventricle. *Circulation research*, *71*(3), 490-502.

Kelly, R. P., Tunin, R., & Kass, D. A. (1992). Effect of reduced aortic compliance on cardiac efficiency and contractile function of in situ canine left ventricle. *Circ Res*, *71*(3), 490-502. https://doi.org/10.1161/01.res.71.3.490

Kolh, P., D'Orio, V., Lambermont, B., Gerard, P., Gommes, C., & Limet, R. (2000). Increased aortic compliance maintains left ventricular performance at lower energetic cost. *Eur J Cardiothorac Surg*, *17*(3), 272-278. https://doi.org/10.1016/s1010-7940(00)00341-9

Lifesciences, E. (2022). *Normal Hemodynamic Parameters and Laboratory Values*. Retrieved 1/29 from https://education.edwards.com/normal-hemodynamic-parameters-pocket-card/1167897#

Linke, W. A., & Fernandez, J. M. (2002). Cardiac titin: molecular basis of elasticity and cellular contribution to elastic and viscous stiffness components in myocardium. *Journal of Muscle Research & Cell Motility*, *23*(5-6), 483-497.

Mack, J. F. (2012). *N-Point Central Differencing*. In https://www.mathworks.com/matlabcentral/fileexchange/36123-n-point-central-differencing

Magosso, E., & Ursino, M. (2001). A mathematical model of CO2 effect on cardiovascular regulation. *American Journal of Physiology-Heart and Circulatory Physiology*, *281*(5), H2036-H2052. https://doi.org/10.1152/ajpheart.2001.281.5.H2036

MathWorks. (2023). *Algebraic Loop Concepts*. Retrieved 6/21/23 from https://uk.mathworks.com/help/simulink/ug/algebraic-loops.html

MathWorks. (2024). MATLAB and Simulink Documentation. In. Web.

Mitchell, G. F. (2008). Effects of central arterial aging on the structure and function of the peripheral vasculature: implications for end-organ damage. *Journal of applied physiology*, *105*(5), 1652-1660.

Mitchell, J. R., & Wang, J.-J. (2014). Expanding application of the Wiggers diagram to teach cardiovascular physiology. *Advances in physiology education*, *38*(2), 170-175.

Moulton, M. J., & Secomb, T. W. (2023). A fast computational model for circulatory dynamics: effects of left ventricle–aorta coupling. *Biomechanics and Modeling in Mechanobiology*, *22*(3), 947-959.

Mulligan, L. J., Mitrev, L., Thrash, J., Folk, D., Exarchakis, A., Ewert, D., & Hill, J. (2024). Evaluation of Vascular Aging on Measures of Cardiac Function and Mechanical Efficiency: Insights from In-Silico Modelling. *Frontiers in Cardiovascular Medicine*, *11*, 1351484.

Mulligan, L. J., Thrash, J., Folk, D., Ciriacy, M., & Ewert, D. L. (2023). Simulated Loss In Arterial Compliance On Measures Of Cardiac Function: A Computational Analysis. *Journal of Cardiac Failure*, *29*(4), 568-569.

Mulligan, L. J., Ungerleider, J., Friedman, A., Sanders, B., Thrash, J., Ewert, D., . . . Hill, J. C. (2024). Evaluation of ventricular–vascular coupling with critical care metrics: An in silico approach. *Physiological Reports*, *12*(3), e15920.

Niederer, S. A., Lumens, J., & Trayanova, N. A. (2019). Computational models in cardiology. *Nat Rev Cardiol*, *16*(2), 100-111. https://doi.org/10.1038/s41569-018-0104-y

Redheuil, A., Yu, W.-C., Wu, C. O., Mousseaux, E., De Cesare, A., Yan, R., . . . Lima, J. A. (2010). Reduced ascending aortic strain and distensibility: earliest manifestations of vascular aging in humans. *Hypertension*, *55*(2), 319-326.

Ricci, D. R., Orlick, A. E., Alderman, E. L., Ingels Jr, N. B., Daughters II, G. T., & Stinson, E. B. (1979). Influence of heart rate on left ventricular ejection fraction in human beings. *The American journal of cardiology*, *44*(3), 447-451.

Schaefer, S., Taylor, A. L., Lee, H. R., Niggemann, E. H., Levine, B. D., Popma, J. J., . . . Hillis, L. D. (1988). Effect of increasing heart rate on left ventricular performance in patients with normal cardiac function. *The American journal of cardiology*, *61*(8), 617-620.

Starling, E. H. (1918). *The Linacre lecture on the law of the heart*. Longmans, Green, & Company.

Suga, H. (1969). Time course of left ventricular pressure-volume relationship under various enddiastolic volume. *Japanese heart journal*, *10*(6), 509-515.

Suga, H. (1970). Time course of left ventricular pressure-volume relationship under various extents of aortic occlusion. *Japanese heart journal*, *11*(4), 373-378.

Ursino, M. (1998). Interaction between carotid baroregulation and the pulsating heart: a mathematical model. *American Journal of Physiology-Heart and Circulatory Physiology*, *275*(5), H1733-H1747. https://doi.org/10.1152/ajpheart.1998.275.5.H1733

Ursino, M., & Magosso, E. (2000). Acute cardiovascular response to isocapnic hypoxia. I. A mathematical model. *American Journal of Physiology-Heart and Circulatory Physiology*, *279*(1), H149-H165. https://doi.org/10.1152/ajpheart.2000.279.1.H149

Ursino, M., & Magosso, E. (2002). A theoretical analysis of the carotid body chemoreceptor response to O2 and CO2 pressure changes. *Respiratory physiology & neurobiology*, *130*(1), 99-110. https://doi.org/10.1016/s0034-5687(01)00335-8

Wiggers, C. J. (1923). *Modern aspects of the circulation in health and disease*. Lea & Febiger.

Zieliński, K., Gólczewski, T., Kozarski, M., & Darowski, M. (2022). Virtual and Artificial Cardiorespiratory Patients in Medicine and Biomedical Engineering. *Membranes*, *12*(6), 548. https://doi.org/10.3390/membranes12060548

APPENDIX A: SIMULINK MODEL SYSTEM PARAMETERS

Table A.1: Tissue Gas Exchange Parameters

Variables		Verification S.M	PV Loop S.M	Ursino Model
Extracellular Tissue Blood Volume [=] ml (Albanese et al., 2016)	V_{Thp}	284	284	284
	V_{Tmp}	31200	31200	31200
	V_{Tbp}	1300	1300	1300
	V_{Tep}	262	262	262
	V_{Tsp}	2673	2673	2673
Metabolic O_2 Consumption Rates [=] ml O_2/min (Albanese et al., 2016)	M_{O2hp}	24	24	24
	M_{O2mp}	51.6	51.6	51.6
	M_{O2bp}	47.502	47.502	47.502
	M_{O2ep}	14.683	14.683	14.683
	M_{O2sp}	108.419	108.419	108.419
Metabolic CO_2 Production Rates [=] ml CO_2/min (Albanese et al., 2016)	M_{CO2hp}	20.16	20.16	20.16
	M_{CO2mp}	43.344	43.344	43.344
	M_{CO2bp}	39.9017	39.9017	39.9017
	M_{CO2ep}	12.3337	12.3337	12.3337
	M_{CO2sp}	91.0720	91.0720	91.0720

Table A.2: Venous Pool Gas Transport and Lung Mechanics Parameters

Variables		Verification S.M	PV Loop S.M	Ursino Model
Venous Respiratory Delay [=] sec (Albanese et al., 2016)	τ_{VL}	10	10	10
Compliances [=] L/cmH_2O (Albanese et al., 2016)	C_{cw}	0.2445	0.2445	0.2445
	C_A	0.2	0.2	0.2
	C_b	0.0131	0.0131	0.0131
	C_l	0.00127	0.00127	0.00127
	C_{tr}	0.00238	0.00238	0.00238
Resistances [=] cmH_2O*sec/L (Albanese et al., 2016)	R_{lt}	0.3369	0.3369	0.3369
	R_{bA}	0.0817	0.0817	0.0817
	R_{tb}	0.3063	0.3063	0.3063
	R_{ml}	1.021	1.021	1.021
Unstressed Air Volumes [=] L air (Albanese et al., 2016)	V_{ul}	0.0344	0.0344	0.0344
	V_{utr}	0.00663	0.00663	0.00663
	V_{ub}	0.0187	0.0187	0.0187
	V_{uA}	0.001263	0.001263	0.001263

Table A.3: Lung-Gas Exchange Parameters

Variables		Verification S.M	PV Loop S.M	Ursino Model
Gas Fractions [=] % (Albanese et al., 2016)	F_{IO2}	0.21037	0.21037	0.21037
	F_{ICO2}	0.000421	0.000421	0.000421
Pressure Loss [=] mmHg (Albanese et al., 2016)	P_{WS}	47	47	47
Environmental Conditions (Albanese et al., 2016)	P_{atm} [=] mmHg	760	760	760
	H_{gb} [=] g/dl	15	15	15
	Sh [=] %	0.017	0.017	0.017
	K	1.2103	1.2103	1.2103
Transport Delay from Lungs to Systemic Circulation [=] sec (Albanese et al., 2016)	τ_{LT}	18	18	18

Table A.4: Left and Right Sides of the Heart Parameters

Variables		Verification S.M	PV Loop S.M	Ursino Model
Volume [=] ml (Ursino, 1998)	V_{ula}	25	25	25
	V_{ulv}	16.77	16.77	16.77
	V_{ura}	25	25	25
	V_{urv}	40.8	40.8	40.8
Resistances [=] mmHg*sec/ml (Ursino, 1998)	R_{la}	0.0025	0.0025	0.0025
	R_{ra}	0.0025	0.0025	0.0025
Viscoelastic Property [=] s/ml (Ursino, 1998)	K_{Rlv}	0.000375	0.000375	0.000375
	K_{Rrv}	0.0014	0.0014	0.0014
Compliances [=] ml/mmHg (Ursino, 1998)	C_{la}	19.23	19.23	19.23
	C_{ra}	31.25	31.25	31.25
Heart Period Activation (Phi) (Ursino, 1998)	k_{sys} [=] s^2	0.075	0.075	0.075
	T_{sys0} [=] sec	0.5	0.5	0.5
Isovolumic Pressure of Ventricles (Ursino, 1998)	$K_{E,lv}$ [=] 1/ml	0.014	0.014	0.014
	$K_{E,rv}$ [=] 1/ml	0.011	0.011	0.011
	$P_{0,lv}$ and $P_{0,rv}$ [=] mmHg	1.5	1.5	1.5

Table A.5: Systemic Circulation Parameters

Variables		Verification S.M	PV Loop S.M	Ursino Model
Blood Volumes [=] ml (Albanese et al., 2016)	V_{usa}	0	0	0
	V_{uhp}	24	24	24
	V_{ubp}	72.13	72.13	72.13
	V_{ump}	105.8	105.8	105.8
	V_{usp}	274.4	274.4	274.4
	V_{uep}	134.64	134.64	134.64
	V_{tvmax}	350	350	350
	V_{tvmin}	50	50	50
	V_{utv}	130	130	130
	V_{uhv}	98.21	98.21	98.21
	V_{ubv}	294.64	294.64	294.64
	V_{umv0}	503.26	503.26	503.26
	V_{usv0}	1435.4	1435.4	1435.4
	V_{uev0}	640.73	640.73	640.73
Compliances [=] ml/mmHg (Albanese et al., 2016)	C_{sa}	0.28	0.28	0.28
	C_{hp}	0.1488	0.1488	0.1488
	C_{bp}	0.5208	0.5208	0.5208
	C_{mp}	0.8184	0.8184	0.8184
	C_{sp}	1.1532	1.1532	1.1532
	C_{ep}	1.0788	1.0788	1.0788
	C_{hv}	2.499	2.499	2.499
	C_{bv}	7.497	7.497	7.497
	C_{mv}	10.997	10.997	10.997
	C_{sv}	42.777	42.777	42.777
	C_{ev}	14	14	14
Static Resistances [=] mmHg*sec/ml (Albanese et al., 2016)	R_{sa}	0.06	0.09	0.06
	R_{hv}	0.224	0.224	0.224
	R_{bv}	0.075	0.075	0.075
	R_{mv}	0.05	0.05	0.05
	R_{sv}	0.038	0.038	0.038
	R_{ev}	0.04	0.04	0.04
	R_{tv0}	0.025	0.025	0.025
Dynamic Resistances [=] mmHg*sec/ml (Albanese et al., 2016)	R_{hpn}	19.71	19.71	19.71
	R_{bpn}	6.6667	6.6667	6.6667
	R_{mp0}	2.106	2.106	2.106
	R_{sp0}	2.49	2.49	2.49
	R_{ep0}	1.655	1.655	1.655

Table A.5: Systemic Circulation Parameters (continued)

Variables		Verification S.M	PV Loop S.M	Ursino Model
Inertance [=] $mmHg*sec^2/ml$ (Albanese et al., 2016)	L_{sa}	$0.22*10^{-3}$	$0.44*10^{-3}$	$0.22*10^{-3}$

Table A.6: Pulmonary Circulation Parameters

Variables		Verification S.M	PV Loop S.M	Ursino Model
Volume [=] ml (Albanese et al., 2016)	V_{upa}	0	0	0
	V_{ups}	0	0	0
	V_{upp}	106.3999	106.3999	106.3999
	V_{upv}	105.6	105.6	105.6
Resistance [=] mmHg*sec/ml (Albanese et al., 2016)	R_{pa}	0.023	0.023	0.023
	R_{ps}	5.2588	5.2588	5.2588
	R_{pp}	0.0909	0.0909	0.0909
	R_{pv}	0.0056	0.0056	0.0056
Compliance [=] ml/mmHg (Albanese et al., 2016)	C_{pa}	0.76	0.76	0.76
	C_{ps}	0.0986	0.0986	0.0986
	C_{pp}	5.7014	5.7014	5.7014
	C_{pv}	25.37	25.37	25.37
Inertance [=] mmHg*sec^2/ml (Albanese et al., 2016)	L_{pa}	0.18*10^-3	0.18*10^-3	0.18*10^-3

Table A.7: ANS Receptor Parameters

Variables		Verification S.M	PV Loop S.M	Ursino Model
Afferent Baroreflex f_{ab} (Ursino, 1998; Ursino & Magosso, 2000)	k_{ab} [=] mmHg	11.76	11.76	11.76
	$f_{ab,max}$ [=] spikes/sec	47.78	47.78	47.78
	$f_{ab,min}$ [=] spikes/sec	2.52	2.52	2.52
	$\tau_{z,b}$ [=] sec	6.37	6.37	6.37
	$\tau_{p,b}$ [=] sec	2.076	2.076	2.076
	P_n [=] mmHg	92	92	92
Afferent Chemoreflex Pathway f_{apc} (Ursino & Magosso, 2002)	A	600	600	600
	B	10.18	10.18	10.18
	K_{O2}	200	200	200
	C_t [=]L CO_2/L blood	0.36	0.36	0.36
	K_{CO2} [=] 1/sec	1	1	1
	K_{stat} [=] 1/sec	20	20	20
	τ_{zh} [=] sec	600	600	600
	τ_{ph} [=] sec	3.5	3.5	3.5
	K_{dyn} [=] 1/sec	45	45	45
	K_{stat} [=] 1/sec	20	20	20
	τ_{pl} [=] sec	3.5	3.5	3.5
Blood-Gas Concentration Detection (Albanese et al., 2016; Ursino & Magosso, 2002)	a_1	0.3836	0.3836	0.3836
	α_1 [=] 1/mmHg	0.03198	0.03198	0.03198
	a_2	1.819	1.819	1.819
	α_2 [=] 1/mmHg	0.05591	0.05591	0.05591
	K_1 [=] mmHg	14.99	14.99	14.99
	β_1 [=] 1/mmHg	0.008275	0.008275	0.008275
	K_2 [=] mmHg	194.4	194.4	194.4
	β_2 [=] 1/mmHg	0.03255	0.03255	0.03255
	C_1 [=] mM/L blood	9	9	9
	$Ca_{O2,max}$ [=] L O_2/L blood	0.2	0.2	0.2
	C_2 [=] mM/L blood	86.11	86.11	86.11
	Z [=] L/mM	0.0227	0.0227	0.0227
Afferent Lung Stretch Receptors	G_{asr} [=] spikes/l*sec	11.76	11.76	23.29 (Ursino & Magosso, 2000) 11.76 (Albanese et al., 2016)
	τ_p [=] sec	2	2	2

Table A.8: Sympathetic ANS Control Parameters

Variables		Verification S.M	PV Loop S.M	Ursino Model
Sympathetic Stimulation Basic Functional Parameters	$f_{es,\infty}$ [=] spikes/sec	2.1	2.1	2.1
	$f_{es,0}$ [=] spikes/sec	16.11	16.11	16.11
	k_{es} [=] sec	0.0675	0.0675	0.0675
	$f_{es,max}$ [=]spikes/sec	60	60	60
Sympathetic Stimulation to Arterial Resistances f_{sp}	$W_{b,sp}$	-1	-1	1 (Ursino & Magosso, 2000)
				-1 (Magosso & Ursino, 2001)
				-1.1375 (Albanese et al., 2016)
	$W_{c,sp}$	5	5	5 (Magosso & Ursino, 2001; Ursino & Magosso, 2000)
				1.716 (Albanese et al., 2016)
	$W_{p,sp}$	-0.34	-0.34	0.34 (Ursino & Magosso, 2000)
				-0.34 (Magosso & Ursino, 2001)
				-0.3997 (Albanese et al., 2016)
	θ_{spn} [=] sec^{-1}	13.32	N/A	13.32 (Magosso & Ursino, 2001)
Sympathetic Stimulation to Veins f_{sv}	$W_{b,sv}$	-1	-1	-1 (Magosso & Ursino, 2001)
				-1.0806 (Albanese et al., 2016)
	$W_{c,sv}$	5	5	5 (Magosso & Ursino, 2001)
				1.716 (Albanese et al., 2016)
	$W_{p,sv}$	-0.34	-0.34	-0.34 (Magosso & Ursino, 2001)
				-0.2907 (Albanese et al., 2016)
	θ_{svn} [=] sec^{-1}	13.32	N/A	13.32 (Magosso & Ursino, 2001)
Sympathetic Stimulation to the Heart f_{sh}	$W_{b,sh}$	-1	-1	1 (Ursino & Magosso, 2000)
				-1 (Magosso & Ursino, 2001)
				-1.75 (Albanese et al., 2016)
	$W_{c,sh}$	1	1	1 (Magosso & Ursino, 2001; Ursino & Magosso, 2000)
	$W_{p,sh}$	0	-1	0 (Magosso & Ursino, 2001; Ursino & Magosso, 2000)
	θ_{shn} [=] sec^{-1}	3.6	N/A	3.6 (Magosso & Ursino, 2001)

Table A.9: Parasympathetic ANS Control Parameters

Variables		Verification S.M	PV Loop S.M	Ursino Model
Parasympathetic ANS Control Signals (Ursino & Magosso, 2000)	$f_{ev,0}$ [=]spikes/sec	3.2	3.2	3.2
	$f_{ev,\infty}$ [=]spikes/sec	6.3	6.3	6.3
	$f_{ab,0}$ [=]spikes/sec	25	25	25
	k_{ev} [=]spikes/sec	7.06	7.06	7.06
	$W_{c,v}$	0.2	0.2	0.2
	$W_{p,v}$	0.103	0.103	0.103
	θv [=]spikes/sec	-0.68	-0.68	-0.68

Table A.10: Hypoxic Response of ANS Parameters

Variables		Verification S.M	PV Loop S.M	Ursino Model
CNS Response offset for f_{sp} (Magosso & Ursino, 2001)	P_{O2nsp} [=]mmHg	30		30
	$k_{isc,sp}$ [=]mmHg	2		2
	χ_{sp} [=] Hz	6		6
	τ_{isc} [=] sec	30		30
	θ_{spn} [=] sec^{-1}	13.32		13.32
	g_{ccsp} [=] 1/(mmHg*sec)	1.5		1.5
	τ_{cc} [=] sec	20		20
	Pa_{CO2n} [=] mmHg	40		40
CNS Response offset for f_{sv} (Magosso & Ursino, 2001)	P_{O2nsv} [=]mmHg	30		30
	k_{iscsv} [=]mmHg	2		2
	χ_{sv} [=] Hz	6		6
	θ_{svn} [=] sec^{-1}	13.32		13.32
	g_{ccsv} [=] 1/(mmHg*sec)	0		0
CNS Response offset for f_{sh} (Magosso & Ursino, 2001)	P_{O2nsh} [=]mmHg	45		45
	k_{iscsh} [=] mmHg	6		6
	χ_{sh} [=] Hz	53		53
	θ_{shn} [=] sec^{-1}	3.6		3.6
	g_{ccsh} [=] 1/(mmHg*sec)	1		1

Table A.11: ANS Regulated States Parameters

Variables		Verification S.M	PV Loop S.M	Ursino Model
Sympathetic Regulated Arterial Resistances (Ursino & Magosso, 2000)	f_{esmin} [=]spikes/sec	2.66	2.66	2.66
	D_{Rep} [=]sec	2	2	2
	G_{Rep} [=]mmHg*s/ml*v	1.94	1.94	1.94
	τ_{Rep} [=] sec	6	6	6
	R_{ep0} [=] mmHg*sec/ml	1.655	1.655	1.655
	D_{Rsp} [=]sec	2	2	2
	G_{Rsp} [=]mmHg*s/ml*v	0.695	0.695	0.695
	τ_{Rsp} [=]sec	6	6	6
	R_{sp0} [=]mmHg*sec/ml	2.49	2.49	2.49
	D_{Rmp} [=]sec	2	2	2
	G_{Rmp} [=]mmHg*s/ml*v	2.47	2.47	2.47
	τ_{Rmp} [=] sec	6	6	6
	R_{mp0} [=]mmHg*sec/ml	2.106	2.106	2.106
Sympathetic Regulated Unstressed Volumes (Ursino & Magosso, 2000)	f_{esmin} [=] spikes/sec	2.66	2.66	2.66
	D_{Vuev} [=]sec	5	5	5
	G_{Vuev} [=]ml/(spikes/sec)	-74.21	-74.21	-74.21
	τ_{Vuev} [=] sec	20	20	20
	$V_{u,ev0}$ [=]ml	640.73	640.73	640.73
	D_{Vusv} [=] sec	5	5	5
	G_{Vusv} [=]ml/(spikes/sec)	-265.4	-265.4	-265.4
	τ_{Vusv} [=] sec	20	20	20
	$V_{u,sv0}$ [=] ml	1435.4	1435.4	1435.4
	D_{Vumv} [=] sec	5	5	5
	G_{Vumv} [=]ml/(spikes/sec)	-58.29	-58.29	-58.29
	τ_{Vumv} [=]sec	20	20	20
	$V_{u,mv0}$ [=]ml	503.26	503.26	503.26
Sympathetically Regulated Elastance (Contractility) (Ursino & Magosso, 2000)	f_{esmin} [=]spikes/sec	2.66	2.66	2.66
	D_{EmaxRV} [=] sec	2	2	2
	G_{EmaxRV} [=]mmHg/ml*v	0.282	0.282	0.282
	τ_{EmaxRV} [=]sec	8	8	8
	E_{maxRV0} [=] mmHg/ml	1.412	1.412	1.412
	D_{EmaxLV} [=]sec	2	2	2
	G_{EmaxLV} [=]mmHg/ml*v	0.475	0.475	0.475
	τ_{EmaxLV} [=]sec	8	8	8
	E_{maxLV0} [=] mmHg/ml	2.392	2.392	2.392

Table A.11: ANS Regulated States Parameters (continued)

Heart Pacing (Ursino & Magosso, 2000)	f_{esmin} [=] spikes/sec	2.66	2.66	2.66
	$D_{T,s}$ [=] sec	2	2	2
	$G_{T,s}$ [=] s/v	-0.13	-0.13	-0.13
	$\tau_{T,s}$ [=] sec	2	2	2
	$D_{T,v}$ [=] sec	0.2	0.2	0.2
	$G_{T,v}$[=] s/v	0.09	0.09	0.09
	$\tau_{T,v}$ [=] sec	1.5	1.5	1.5
	T_0 [=] sec	0.58	0.58	0.58

Table A.12: Respiratory Control Parameters

Variables		**Verification S.M Parameter**	**PV Loop S.M Parameter**	**Ursino Parameter**
Respiratory Pressure [=] cmH_2O (Albanese et al., 2016)	$P_{mus,min}$	-5	-5	-5
Respiratory Rate (Albanese et al., 2016)	RR0 [=] breath/min	12	12	12
	T [=] sec	5 (Constant for Sim)	5 [=] sec (Constant for Sim)	Dynamic
	IE_{ratio}	0.6	0.6	0.6
	Tau	$T_E/5$	$T_E/5$	$T_E/5$
	T_I[=] sec	1.97	1.97	Dynamic
	T_E [=] sec	3.03 (Constant for Sim)	3.03 (Constant for Sim)	Dynamic

Table A.13: Autoregulation Parameters

Variables		Verification S.M Parameter	PV Loop S.M Parameter	Ursino Parameter
Gas Concentrations [=] mL (gas)/ mL (blood) (Ursino & Magosso, 2000)	C_{vhO2n}	0.11	0.11	0.11
	C_{vbO2n}	0.14	0.14	0.14
	C_{vmO2n}	0.155	0.155	0.155
Normalized Resistance [=] mmHg*sec/mL (Albanese et al., 2016)	R_{hpn}	19.71	19.71	19.71
	R_{bpn}	6.6667	6.6667	6.6667
Autoregulation Gains [=] mL blood/ mL O_2 (Ursino & Magosso, 2000)	G_{hO2}	35	30	35
	G_{bO2}	10	10	10
	G_{mO2}	30	30	30
Time Delays [=] sec (Ursino & Magosso, 2000)	τ_h	10	10	10
	τ_b	10	10	10
	τ_m	10	10	10

APPENDIX B: LIST OF SIMULINK MODEL I/O WAVEFORMS

Table B.1: List of Hemodynamic Waveforms Within Simulink Model

Waveform	Meaning
BP	Arterial Blood Pressure
DBP	Diastolic Blood Pressure of the Systemic Arteries
EDV	End Diastolic Volume of the Left Ventricle
F_{il}	Blood Flow into the Left Ventricle
F_{ir}	Blood Flow into the Right Ventricle
F_{la}/Q_{pv}	Blood Flow to the Left Atrium/Blood Flow to the Pulmonary Vein
F_{or}	Blood Flow out of the Right Ventricle
F_{pa}	Blood Flow through the Pulmonary Artery
F_{ra}/Q_{tv}/VR	Blood Flow to the Right Atrium/Flow through the Thoracic Veins/Venous Return
F_{sa}	Blood Flow of the Systemic Arteries
HMP	Hydromotive Pressure
LVP	Left Ventricular Pressure
LVV	Left Ventricular Volume
MAP	Mean Arterial Blood Pressure
$P_{arterial}$	Equivalent Parallel Arterial Pressure
P_{la}/LaP	Left Atrial Pressure
$P_{max,lv}$	Maximum Isovolumic Pressure of the Left Ventricle
P_{pa}/PAP	Pulmonary Artery Pressure
P_{sa}/AoP	Blood Pressure of the Systemic Arteries/Aortic Pressure
$P_{tm,\ tv}$	Transmural Pressure of the Thoracic Veins
P_{tv}	Blood Pressure of the Thoracic Veins
Q_{jp}	Arterial Blood Flow through a Compartment
Q_{pp}	Blood Flow through the Alveolar Capillaries
Q_{ps}	Blood Flow through the Pulmonary Shunt
RAP	Right Atrial Pressure
R_{bp}	Autoregulated Cerebral Arterial Resistance
R_{hp}	Autoregulated Coronary Arterial Resistance
R_{mp}	Autoregulated Skeletal Arterial Resistance
R_T	Total Peripheral Resistance
RVP	Right Ventricular Pressure
RVV	Right Ventricular Volume
SBP	Systolic Blood Pressure of the Systemic Arteries
SV_l	Left Ventricular Stroke Volume
SV_r	Right Ventricular Stroke Volume
VCP	Vena Caval Pressure

Table B.1: List of Hemodynamic Waveforms Within Simulink Model (continued)

Waveform	Meaning
V_{jp}	Arterial Blood Volume within a Compartment
V_{pp}	Blood Volume within the Alveolar Capillaries
V_{ps}	Blood Volume within the Pulmonary Shunt
V_{pv}	Blood Volume within the Pulmonary Vein
$\varepsilon(t)$	Time-Varying Elastance of the Left Ventricle

Table B.2: List of Respiration and Blood-Gas Exchange Waveforms within Simulink Model

Waveform	Meaning
$C_{a,CO2}$	Concentration of CO_2 in the Arterial Blood
$\widetilde{C_{a,CO2}}$	Time Delayed Concentration of CO_2 in the Arterial Blood
$C_{a,O2}$	Concentration of O_2 in the Arterial Blood
$\widetilde{C_{a,O2}}$	Time Delayed Concentration of O_2 in the Arterial Blood
$C_{jp,CO2}$	Arterial Compartment Carbon Dioxide Concentration
$C_{jp,O2}$	Arterial Compartment Oxygen Concentration
$C_{pp,CO2}$	Concentration of CO_2 within Alveolar Capillaries
$C_{pp,O2}$	Concentration of O_2 within Alveolar Capillaries
$C_{v,CO2}$	Concentration of CO_2 in the Venous Blood
$\widetilde{C_{v,CO2}}$	Time Delayed Venous Concentration of CO_2
$C_{v,O2}$	Concentration of O_2 in the Venous Blood
$\widetilde{C_{v,O2}}$	Time Delayed Venous Concentration of O_2
$F_{A,CO2}$	Gas Fraction of CO_2 within the Alveolar Space
$F_{A,O2}$	Gas Fraction of O_2 within the Alveolar Space
$F_{D,CO2}$	Gas Fraction of CO_2 within the Dead Space
$F_{D,O2}$	Gas Fraction of O_2 within the Dead Space
$P_{a,CO2}$	Partial Gas Pressure of CO_2 in the arteries
$P_{a,O2}$	Partial Gas Pressure of O_2 in the arteries
$S_{a,\,O2}$/ $S_{p,\,O2}$	Saturation of Arterial Oxygen

Table B.3: List of Lung Mechanics Waveforms within Simulink Model

Waveform	Meaning
P_A	Air Pressure of the Alveolar Sac Region
P_b	Air Pressure of the Bronchial Tubes
P_l	Air Pressure of the Larynx
P_{mus}	Pressure of Respiratory Muscles
P_{pl}	Pressure of the Pleural Cavity
P_{tr}	Air Pressure of the Trachea
RR	Respiratory Rate
V_A	Air Volume of the Alveolar Sac Region
$\dot{V}_A$	Airflow through the Alveolar Sac Region
V_b	Air Volume of the Bronchial Tubes
V_D	Total Volume of the Dead Space
$\dot{V}$	Total Respiratory Airflow
V_l	Air Volume of the Larynx
V_L	Total Volume of the Lungs
V_{L_T}	Tidal Volume of the Lungs
V_{tr}	Air Volume of the Trachea

Table B.4: List of ANS Waveforms within Simulink model

Waveform	Meaning
fab	Frequency of Afferent Baroreceptors
fap	Frequency of Afferent Lung Stretch Receptors
fapc	Frequency of Afferent Peripheral Chemoreceptors
fev	Frequency of Parasympathetic Stimulation to the Heart
fsh	Frequency of Sympathetic Stimulation to the Heart
fsp	Frequency of Sympathetic Stimulation to the Peripheral Resistance
fsv	Frequency of Sympathetic Stimulation to the Veins
θ_s	Sympathetic Offset Term
θ_v	Parasympathetic Offset Term

Table B.5: List of ANS Regulated Waveforms within Simulink model

Waveform	Meaning
$E_{max,lv}$	Maximum Elastance of the Left Ventricle
$E_{max,rv}$	Maximum Elastance of the Right Ventricle
φ	Activation Function of the Heart (Phi)
R_{ep}	Extrasplanchnic Arterial Resistance
$R_{mp,n}$	Nominal Skeletal Muscle Resistance
R_{sp}	Splanchnic Arterial Resistance
T	Heart Period
T_{sys}	Duration of Systole
V_{uev}	Unstressed Volume of the Extra Splanchnic Veins
V_{umv}	Unstressed Volume of the Skeletal Muscle Veins
V_{usv}	Unstressed Volume of the Splanchnic Veins

APPENDIX C: SIMULINK MODEL SYSTEM DESCRIPTION

C.1 Overview of the Unified Cardiopulmonary Model

The multiple cardiovascular and pulmonary models designed by Ursino et al. used a variety of phenomenological and constitutive equations to represent the following systems: 1) the left and right side of the heart, 2) systemic circulation through five vascular compartments, 3) tissue gas-exchange, 4) venous gas transport, 5) lung mechanics, 6) pulmonary hemodynamic circulation and lung-gas exchange, and 7) ANS stimulation and regulation. Phenomenological equations represent physics or biological phenomena using a derived mathematical model. Constitutive equations represent the fundamental mechanical function and the relationship between two dynamically varying quantities (i.e., hemodynamic pressure and blood flow) and incorporate fundamental laws of physics in their creation. Phenomenological and constitutive equations are represented using derived functions or ordinary differential equations (ODE). Equation parameters are derived using measured data, and a model fit can be estimated using either a statistical or dynamic approach, depending on the data type and mathematical model. Each Ursino cardiovascular and pulmonary system model takes a constitutive and phenomenological approach to represent the hemodynamic, gas-exchange, lung mechanical, and autonomic reflex regulation system function using multiple mathematical functions or differential equations based on conservation laws of mass, conservation of energy, or mass-flow balance. The function of each system model varies depending on the lumped parameters of each constitutive or phenomenological equation. A parameter can represent a passive, constant element or time-varying behavior of a known energy-producing or storing quantity. Many principles of control theory, such as negative feedback regulation and control laws, are employed throughout the multiple models, especially in the ANS. Equations designed by Ursino et al.

interlink together to form the function of a system, and these systems can link together to form a cardiopulmonary system. This next section will briefly outline the function of each system modeled by Ursino et al. above and discuss how the systems connect to create a unified cardiopulmonary model. The reader should refer to the following cited model papers to understand the CV and pulmonary modeling approach of Ursino et al. in depth.

C.2 Right and Left Sides of the Heart

The left and right heart model equations, designed by Mauro Ursino, represent its hemodynamics using an ideal electrical analog system that calculates total pressure, volume, and blood flow through the atria, ventricles, and valves each linked together using a Windkessel principle (Ursino, 1998). Hemodynamic pressure, volume, and blood flow in a heart region are equivalent to the voltage, charge, and current of the electrical analog model. Each region of the heart functions using a two-element electrical circuit system with constant resistance and compliance to determine the total blood pressure, the flow of blood through these regions, and the total volume at any instantaneous point in time.

Within the broader cardiopulmonary model, the primary inputs to the heart that drive its hemodynamics are the systemic venous return of blood ($F_{ra} = Q_{tv}$), the deoxygenated concentration of blood ($C_{v,\,gas}$) from the venous pool gas transport, and ANS stimulation from the sympathetic (fsh) and parasympathetic (fev) systems sent to the right atrium. The primary outputs from the heart are the arterial concentration of oxygenated blood ($C_{a,\,gas}$) from the pulmonary circulation, the partial gas pressure of oxygen ($P_{a,\,O2}$) and carbon dioxide ($P_{a,\,CO2}$) within that concentration, and the hemodynamics of blood flow through the aortic valve (Albanese et al., 2016; Ursino, 1998). Right and left ventricular pressure acts as the primary driver of the heart and is modeled using phenomenological equations that compute their

respective isometric pressure and viscous resistive losses(Ursino, 1998). The timing of these ventricular pressure waveforms is driven by ANS stimulation, that dictates the duration of filling and contraction. A valve model consisting of a pressure gradient and resistive element separates and calculates the flow through two successive heart regions.

C.3 The Systemic Vascular Circulatory System

The systemic vascular circulation electric analog model begins with the flow from the aortic valve (Fol) entering the aortic arch region, which calculates the pressure of the systemic arteries (Psa) and the blood flow (Fsa) that will split into the coronary, brain, skeletal muscle, splanchnic, and extra-splanchnic vascular compartments (denoted by 'j'), consisting of an arterial region (represented by subscript' p') and a venous section (designated by subscript' v') connected in parallel (Albanese et al., 2016). Inputs into the system are the arterial oxygenated blood ($C_{a,\ gas}$), partial gas pressures ($P_{a,\ O2}$ and $P_{a,\ CO2}$), the flow of blood out the aortic valve (Fol), ANS regulated arterial resistances (R_{sp} and R_{ep}), autoregulated arterial resistances (R_{hp}, R_{bp}, R_{mp}), and pleural pressure from the lungs (P_{pl}). The outputs from the systemic circulation are the arterial and venous blood flow (Qjp and Q_{jv}), blood volume (V_{jp} and V_{jv}), and pressure (P_{jp} and P_{jv}) for each compartment as well as the flow through the thoracic veins connected to the right atrium (Qtv = Fra). Modeling of the system equations went in the order of the blood flow through the arterial and venous system, starting with the systemic arterial hemodynamics and then splitting along the parallel path of each vascular compartment representing the arterial and venous hemodynamics. The flow out of the aorta (F_{ol}) enters into the aortic arch region of the model, which determines the total aortic pressure (P_{sa}) and the flow of blood (F_{sa}) that will enter the coronary brain, skeletal muscle, splanchnic, and extra-splanchnic vascular compartments (Albanese et al., 2016). An ODE system containing static hemodynamic resistance (Rsa),

compliance (C_{sa}), and fluid inertance (L_{sa}) parameters represents the mechanics of aortic pressure (Psa) and the flow of blood into the systemic arteries (Fsa). The configuration of the systemic circulation has the systemic arteries region acting as the source and the five vascular compartments connected in a parallel branch electrical circuit. The parallel connection means that the arterial pressures of the coronary, brain, skeletal muscle, splanchnic, and extra-splanchnic are equal ($P_{hp} = P_{bp} = P_{mp} = P_{sp} = P_{ep}$) and solved in an ODE based on the principle of equivalent arterial compliance and a summation of blood flow. Arterial pressure drives the flow through each branch's arterial and venous regions, each having its own ODE and complimentary equations to compute hemodynamics. Each vascular branch of the systemic circulation divides into arterial and venous components connected in series with varying mechanical and regulatory mechanisms. Blood flow through the arteries uses a varying arterial-venous pressure gradient that interacts with a hemodynamic resistance controlled through ANS stimulation and local-effect autoregulation, which varies depending on arterial blood-gas concentration (C_a). The venous blood flow functions based on ANS-regulated unstressed volumes, pressure calculated based on the arterial blood flow in the preceding region, and the influence of hemodynamic transmural pressure from the movement of the lungs and increase in thoracic cavity pressure (P_{tv}). Venous blood flow serves as the primary remover of waste products of metabolism in the form of residual oxygen and generated carbon dioxide. The flow of blood from the venous region meets at a single nodal pressure point (P_{tv}), where they add together in the thoracic veins (Q_{tv}) for return to the right atrium of the heart (F_{ra} is equivalent to Q_{tv}).

C.4 Tissue Gas Exchange

Arterial blood contains a concentration of affixed oxygen (O_2) and carbon dioxide (CO_2) that are circulated throughout the body's tissues to fuel metabolism and normal systemic

function. The tissue gas exchange model represents the mechanism of delivering oxygen and carbon dioxide concentrations, $C_{a,\,O2,}$ and $C_{a,\,CO2,}$ respectively, from the arterial side using a mass-flow balance equation for each vascular compartment. Each given compartment of the tissue gas exchange model functions as a lumped system with a constant tissue volume ($V_{T,\,jp}$ where jp is a given arterial compartment), a constant oxygen consumption ($M_{O2,\,jp}$), and carbon dioxide production rate ($M_{CO2,\,jp}$)(Albanese et al., 2016). The model uses two ODEs for a vascular region to calculate the total concentration of arterial oxygen ($C_{jp,\,O2}$) and carbon dioxide ($C_{jp,\,CO2}$) using the total inflow of arterial blood (Q_{jp}) delivering a difference of arterial gas concentration ($C_{a,\,gas} – C_{jp,\,gas}$), the total combined arterial (V_{jp}) and tissue blood volume ($V_{T,\,jp}$), and the metabolic production rate ($M_{\,gas,\,jp}$). Arterial gas concentration represents a volume of gas per volume of the blood delivered to a compartment. The blood inflow and the gas consumption or production rate set the transfer rate of a gas concentration. This system calculates the remaining concentration of arterial gas for oxygen ($C_{jp,\,O2}$) and carbon dioxide ($C_{jp,\,CO2}$) for a vascular region. After calculating the arterial tissue-gas concentration for a given region, it will connect with the venous system circulation on its same vascular branch, which handles the transportation of CO_2 waste.

C.5 Venous Gas Transport

Gas concentrations for the arteries of each vascular compartment ($C_{jp,\,gas}$) connect with a corresponding venous gas concentration ($C_{jv,\,gas}$) model connected in series to determine the remaining blood-oxygen and produced carbon dioxide through a region and then calculate the total venous gas transported to the heart via the thoracic vein blood flow (Q_{tv} is equivalent to F_{ra}) (Albanese et al., 2016). Two differential equations determine the total venous concentration of oxygen ($C_{jv,\,O2}$) and carbon dioxide ($C_{jv,\,CO2}$) in a compartment and represent the

phenomenological process of gases affixing to blood within the capillaries. Venous gas concentration for a region depends on the input blood-gas concentration from the arteries ($C_{jp,\ gas}$), the arterial blood flow rate through that region, and the total blood volume within the venous portion of the vascular branch. When each concentration is determined, the pooled oxygen and carbon dioxide gas concentrations within the thoracic veins are determined using a multi-element mass-flow balance differential equation for the five vascular compartments. Blood flow for the five venous compartments (Q_{jv}) delivers a concentration of venous gas ($C_{v,\ gas} - C_{jv,\ gas}$) that will summate into the pool of thoracic vein blood volume (V_{tv}) pumped into the right atrium of the heart (F_{ra}). The physiological process of affixing oxygen and carbon dioxide to the blood creates a time delay before that concentration reaches the thoracic veins and pulmonary circulation. This delay is represented by taking the gas concentration signal and time-delaying it by a set period (τ_{VL}) for all points in time in the model simulation, making the gas concentration of venous blood $\widetilde{C_{v,gas}}$.

C.6 Local Effect Autoregulation

Arterial hemodynamics are influenced by their resistances which vary based on vessel diameter and can be regulated by either ANS electrical stimulation or local gas-effect autoregulation(Ursino & Magosso, 2000). The coronary, brain, and skeletal muscle tissue require a consistent oxygen concentration via blood volume and flow to fuel metabolism and survival in these vital organs. Therefore, a rapid local effect autoregulation is required to maintain the oxygen supply to adjust hemodynamic resistance. Local effect autoregulation varies resistance based on the blood-gas concentrations of a venous region by dilating under high carbon dioxide concentration or constricting under high oxygen conditions(Ursino & Magosso, 2000). Ursino et al. modeled this system by directly inputting the venous blood-gas oxygen concentrations from

the coronary, brain, and skeletal muscle regions along with an ANS-regulated nominal set point for the skeletal muscle resistance. The system directly outputs arterial resistances for the corresponding vascular compartments (R_{hp}, R_{bp}, and R_{mp}), which get fed into the systemic circulation. Implementing these equations involved programming oxygen blood-gas concentration transduction mechanism differential equations (x_j). These equations output a stimulus-response (x_j) depending on the venous concentration of oxygen relative to a nominal amount ($C_{vj,\,O2} - C_{vj,\,O2n}$), the static gain coefficient ($G_{j,\,O2}$), and the time constant (τ_j). The stimulus response is then input into an equation that directly compares the nominal arterial resistance ($R_{jp,\,n}$) to determine the arterial resistance of a compartment (R_{jp}). If the oxygen concentration is below the nominal amount, this increases the stimulus response (x_j) and decreases arterial resistance (R_{jp}) while higher oxygen concentrations provoke an inverse response in Rjp. This directly inputs into the arterial compartments of the coronary, cerebral, or skeletal muscle and dictates the flow of blood through each branch.

C.7 Lung Mechanics

The mechanical function of the lungs operates through the contraction of the diaphragm respiratory muscles to draw outside air inwards through the open airway (ao), larynx (l), trachea (tr), the bronchial tubes (b), and then down to the alveolar sacs (A) using negative pressure process to reoxygenate the blood and then expel metabolic waste out the lungs during the relaxation of the muscles. Ursino et al. modeled lung function using an electrical analog ODE model of a two-voltage source circuit with resistors and capacitors representing the driving pressure sources, airway resistance, and the reserve of air located in each region of the respiratory system(Albanese et al., 2016). The two pressure sources of the model are ventilation pressure (P_{vent}) and respiratory muscle pressure (P_{mus}) represent the external atmospheric

pressure and pressure generated by the diaphragm muscle contracting from neurological stimulation, respectively. Within the programming of the Simulink model, P_{vent} is assumed to be constant, at the standard sea-level atmospheric pressure of 1 atm (760 mmHg), making P_{mus} the driving dynamic pressure. As the diaphragm (Pmus) contracts and relaxes it interacts with the compliance of the thoracic cavity (C_{CW}) in the form of an applied pressure that is divided into the pericardial cavity containing the heart and the pleural cavity which holds the alveolar sacs, bronchial tubes, and trachea of the lungs. The pleural cavity pressure (P_{pl}) regulates the direction of airflow through the three parallel electrical circuit branches of the alveoli, bronchial, and tracheal regions. Total airflow into the respiratory system ($\dot{V}$) varies the volume of air at each region of the system at any instantaneous point in time. This total airflow can be further divided into the site of gas exchange in the lungs in the alveoli ($\dot{V}_A$) and the remaining respiratory regions called the dead space ($V_{.D.}$). The lung mechanics model directly connects with the hemodynamic system through the pressure applied to the thoracic veins (P_{tv}) via the pleural pressure (P_{pl}) and directly controls the gas-exchange respiration rate within the lungs by removing carbon-dioxide within the blood and reoxygenating the hemoglobin before returning to the left heart.

C.8 Pulmonary Circulation

The function of the pulmonary circuit is to take the deoxygenated blood concentrations from the venous gas transport that are pumped by the right ventricle and circulate it through the point of lung-gas exchange. Ursino's pulmonary circulatory model was built on multiple iterations and includes the pulmonary arteries (pa), the circulation through the peripheral capillaries of the lung gas exchange system (pp), the blood that isn't exchanged and is shunted (ps), and then the combination of the two blood streams which pass through the pulmonary vein and into the left atrium (P_{pv} is equivalent to P_{la})(Albanese et al., 2016; Ursino, 1998; Ursino &

Magosso, 2000). The inputs into the system are the flow of blood through the pulmonary valve (For), the time-delayed venous concentration of oxygen ($\widetilde{C_{v,O2}}$) and carbon dioxide ($\widetilde{C_{v,CO2}}$) within the blood. The outputs of the system are the time-delayed arterial concentrations of oxygen and carbon dioxide within the blood ($\widetilde{C_{a,O2}}$ and $\widetilde{C_{a,CO2}}$), the partial gas pressure or tension each gas exerts within the blood ($P_{a,\,O2}$ and $P_{a,\,CO2}$), and the flow of blood into the left atrium (Q_{pv} is equivalent to Q_{la}). The pulmonary artery region functions as a three-element electrical circuit model that models flow, pressure, and volume of the region based on a compliance (C_{pa}), inertance (L_{pa}), and resistance (R_{pa}) parameters and the interaction of applied transmural pleural cavity pressure (P_{pl}). From the artery, the circulation model of the blood separates into two parallel electrical circuit model regions, the portion of the peripheral arterial vessels and capillaries where lung gas exchange occurs (Q_{pp}) and the blood that does not exchange gasses, represented as a pulmonary shunt (Q_{ps}). The amount of blood that passes through the pulmonary peripheral region and exchanges gasses, changes the saturation of oxygen in the blood ($S_{a,O2}$) and the partial gas pressure/tension for oxygen ($P_{a,\,O2}$) and carbon dioxide ($P_{a,\,CO2}$) within the systemic arteries and delivered in the tissue-gas exchange.

C.9 Lung Gas Exchange

The lung gas exchange system removes waste carbon dioxide blood-gas concentrations ($\widetilde{C_{v,O2}}$ and $\widetilde{C_{v,CO2}}$) from venous blood flow to the pulmonary capillaries (Q_{pp}) that connect to the alveolar sacs (Albanese et al., 2016). A dissociation process removes carbon dioxide from the hemoglobin and affixes oxygen concentrations to the blood ($C_{a,\,O2}$ and $C_{a,\,CO2}$) that will reoxygenate the systemic tissues. The model developed by Ursino et al. represented this gas exchange process using a series of mass-flow balance equations that incorporate outputs from the lung mechanics, pulmonary circulation, and blood-gas concentrations from the venous system to

remove waste carbon and replace it with inspired oxygen(Albanese et al., 2016). Simulink modeling started with the dead space gas fraction equations ($F_{D,\,O2}$ and $F_{D,\,CO2}$), which function in a logical timing operation based on mechanical airflow ($\dot{V}$) that defines inhalation of inspired oxygen during the positive mechanical airflow of inhalation and gas exchange occurring during exhalation as the direction of flow reverses ($-\dot{V}$). Blood-gas disassociation equations ($C_{pp,\,gas}$) were programmed to represent the amount of carbon dioxide and oxygen that can be removed or affixed, respectively, for a given volume of blood.

Blood-gas disassociation results connect to mass-flow balance alveolar gas fraction equations that take a given volume of blood within the pulmonary capillaries (V_{pp}), the flow of blood from the pulmonary arteries (Q_{pa}), and the dead space gas fractions ($F_{D,\,O2}$ and $F_{D,\,CO2}$) to determine alveolar sac carbon dioxide and oxygen Percents ($F_{A,\,O2}$ and $F_{A,\,CO2}$). Finally, the arterial blood-gas concentration ($C_{a,\,gas}$), partial pressures ($P_{a,\,gas}$), and total saturation of O_2 ($S_{a,\,O2} = S_{p,\,O2}$) equations each use the gas fractions of the alveolar sac region to determine the final output of this system transported via the pulmonary vein (Q_{pv}) to the left side of the heart (F_{la}). The delay in transporting a given blood-gas concentration from alveolar sacs to the systemic tissues is represented in the Simulink model using a time delay using parameters published by Ursino et al (Albanese et al., 2016).

C.10 Autonomic Nervous System Stimulation and Control

The autonomic nervous system acts as the rapid regulation system of the body by taking afferent electrical signals from sensory receptors, processing them into a response in the central nervous system, and then enacting a regulatory stimulus in the form of an efferent electrical signal targeted to a select region of the body. Ursino et al. developed multiple iterations of a mathematical ANS model that added new sensory receptors, varied parameter values to simulate

differing conditions in the body, and new regulated control states. The form of each model followed a consistent structure with a sensory or afferent signals, the sympathetic and parasympathetic efferent signal regulation, and ANS regulated states of the model. A major goal of implementing this system was to provide the greatest sensory information and ANS regulation to best represent the physiologic capabilities of autonomic regulation.

The sensory region consists of a carotid baroreceptor (f_{ab}) that monitors the pulsatility and strength of aortic pressure (AoP), a peripheral body chemoreceptor (f_{apc}) that monitors blood gas concentration ($C_{a,\,O2}$ and $C_{a,\,CO2}$) and tensions ($P_{a,\,O2}$ and $P_{a,\,CO2}$) of the arteries, a lung stretch receptor (fap) that monitors the tidal volume of air within the lungs (V_{L_T}) during mechanical respiration. Implementing the carotid baroreceptor equations involved an ODE that measured the dynamic behavior of AoP that was then directly input into a static characteristic function that output an electrical stimulation signal in terms of spikes per second(Magosso & Ursino, 2001; Ursino, 1998). The chemoreceptor equations are represented as a multistage linked differential and mathematical function system that determines the static response of the chemoreceptor due to the partial gas contributions of O_2 and CO_2 within a concentration of arterial blood and then a dynamic response to the rapid changes in arterial CO_2 due to respiration(Ursino & Magosso, 2002). The output of the chemoreceptor equation (f_{apc}) and the partial pressure of CO_2 in the arteries directly feed into a respiratory muscle pressure system that directly computes Pmus and feeds it into the lung mechanics system. Pulmonary lung stretch receptors are based on a derived linear ODE model that proportionally responds to changes in lung volume as a result of the movement of Pmus during inhalation and exhalation(Ursino & Magosso, 2000).

The effector regulation region of the model represents the sympathetic and parasympathetic systems of the ANS and are broken down into regions of regulation, starting

with the sympathetic stimulation to the peripheral arteries (f_{sp}), veins and unstressed volumes (f_{sv}), and cardiac nerves and muscle fibers (f_{sh}) while the parasympathetic system directly inputs into the cardiac fibers to regulate heart period (f_{ev}) (Magosso & Ursino, 2001; Ursino & Magosso, 2000). Both the sympathetic and parasympathetic model equations assume that their activities are a monoexponential function made of a weighted summation of afferent sensory signals. The response from each signal is directly shifted based on an offset term that varies with CNS response to hypoxia.

Regulated states of the model include the peripheral resistances, unstressed volumes of the veins, and the stimulation to the heart by the ANS model equations. The peripheral resistance, unstressed volumes, and cardiac fiber regions are directly regulated by the sympathetic stimulation to the arteries (f_{sp}), sympathetic stimulation to the veins (f_{sv}), and sympathetic innervation to the heart (f_{sh}) and the parasympathetic inhibition from the vagal nerve (f_{ev}), respectively. Each equation is designed based on an assumed latency delay in an ANS signal reaching its regulated state, a monotonic logarithmic static function, and a low-pass filter ODE designed to represent the dynamic shift that will occur in this quantity as stimulation changes. When the total dynamic response is calculated from a state it is compared to its nominal or basal value for that state which is in the form of a hemodynamic resistance, unstressed volume, elastance, or heart period. The heart period response equation differs in that it determines the change in sympathetic and parasympathetic stimulation (ΔT_s and ΔT_V) based on their own separated logarithmic equation and ODE pathway and then sums them together with the nominal period value (T_0). Increases in sympathetic activity to the heart (f_{sh}) are assumed to decrease period while the increase in parasympathetic stimulation (f_{ev}) increases the total period and a decrease in heart rate. The instantaneous heart period is then fed into an activation function

that determines the proportion of a beat in systole or in diastole and the point in in which a ventricle contracts or relaxes.

APPENDIX D: MATLAB CODE

D.1 Verification MATLAB Code

D.1.1. Extract Data Points from MATLAB Figure: MathWorks File Exchange (Danz, 2020)

```
function [content, dtHandle] = getDataTips(h, outputFormat)
% Source: <a href =
"https://www.mathworks.com/matlabcentral/fileexchange/82038-
getdatatips-get-data-tip-text-and-handles">getDataTips</a>
% Author: <a href =
"https://www.mathworks.com/matlabcentral/profile/authors/3753776-adam-
danz">Adam Danz</a>

% Copyright (c) 2020  All rights reserved

% Version History
% vs 1.0.0   201029   Initial update to FEX.
% vs 1.0.1   201029   Added hyperlinks to doc and license info.

%% Input validity
narginchk(0,2)
assert(~verLessThan('Matlab', '8.4'), 'GETDTCONTENT:OldeRelease', ...
    '%s() is not supported in Matlab r2014a or earlier.', mfilename) %
(see [3])
if nargin==0 || isempty(h)
    h = gcf();
else
    assert(all(ishghandle(h)), 'GETDTCONTENT:InvalidHandles', ...
        'H must be vector of valid graphics handles to figures or
axes.')
end
if nargin < 2 || isempty(outputFormat)
    outputFormat = 'cell';
else
    validatestring(outputFormat,{'cell','char'}, mfilename,
'outputFormat');
end
nout = nargout();

%% Extract datatip content
OUT.content = cell(size(h));
OUT.dtHandle = OUT.content;
for i = 1:numel(h)
    [OUT.content{i}, OUT.dtHandle{i}] = getDT(h(i), outputFormat,
nout);
```

```
end

% Assign outputs
if nout>0
    content = OUT.content;
    dtHandle = OUT.dtHandle;
end

function [dtContent, pdth] = getDT(handle, outputFormat, nout)
% HANDLE is a scalar graphics handle (figure or axes)
% OUTPUTFORMAT is either 'char' or 'cell'.
% NOUT is number of output args to main func.
% DTCONTENT is a cell array of all data tip content within HANDLE.
% PDTH is an nx2 array of handles to n data tips in 'handles'. Column
%   1 are PointDataTip handles. Column 2 are DataTip handles in newer
%   releases of Matlab or graphics placeholders in older releases.

% Get figure handle for h
fig = ancestor(handle,'figure');

% Is the input handle the fig handle?
isFigHandle = isequal(fig, handle);

% Get all pointDataTip handles in figure (see [1,4])
figObjs = findall(fig);
pdth =
figObjs(arrayfun(@(h)isa(h,'matlab.graphics.shape.internal.PointDataTi
p'),figObjs));

% Get all datatip handles in figure (see [1,4])
dth = findall(fig, 'Type', 'DataTip');
if isempty(dth)
    pdth(:,2) = gobjects(size(pdth));
else
    pdth(:,2) = dth;
end

% Remove any datatip handles that do not belong to input axes (if
handle refers axes) (see [2])
if ~isempty(pdth)
    selectedAncestor = ismember(pdth(:,1), findall(handle));
    pdth(~selectedAncestor,:) = [];
end

% Display content of all data tips separated by a new line for each
data tip (see [1])
```

```
if isempty(pdth)
    dtContent = {};
elseif isprop(pdth(1,2),'Content')
    % for DataTip objs
    dtContent = {pdth(:,2).Content}'; % col vec
else
    % for PointDataTip objs, we want to access the string property. In
some releases there is
    % an interpreter property that needs to temporarily be set to
'none'.
    if isprop(pdth(1,1), 'Interpreter')
        origInterps = get(pdth(:,1), 'Interpreter');
        set(pdth(:,1), 'Interpreter', 'none');
    end
    if size(pdth,1)==1
        dtContent = cellstr({get(pdth(:,1),'String')});
    else
        dtContent =
cellfun(@cellstr,get(pdth(:,1),'String'),'UniformOutput',false); % col
vec
    end
    if isprop(pdth(1,1), 'Interpreter')
        set(pdth(:,1), {'Interpreter'}, origInterps);
    end
end

if nout==0
    % Print results to command window if there are no outputs
    figLink = ['<a href="matlab: figure(',num2str(fig.Number),')
">',sprintf('Figure %d',fig.Number),'</a>'];
    if isFigHandle
        addendum = '';
    else
        addendum = 'specified axes within';
    end
    if ~isempty(pdth)
        dtArray = reshape([dtContent,repelem({'------
'},size(pdth,1),1)]',[],1);
        dtArrayCol = vertcat(dtArray{:});
        fprintf('Data tips found in %s %s:\n',addendum,figLink)
        disp(char(strcat(repmat({'   '},numel(dtArrayCol),1),
dtArrayCol)))
    else
        fprintf('No data tips found in %s %s.\n',addendum,figLink)
    end
else
```

```
    % Format data tip content
    if strcmpi(outputFormat, 'char')
        dtContent = cellfun(@char,dtContent,'UniformOutput',false);
    end
end

%% Footnotes
% [1] For Matlab r2018b (I think) and later, data tips produce
'DataTip' and 'PointDataTip'
%   objects but only the latter are returned for earlier releases.
DataTip objs have a
%   'Content' property containing the data tip string but PointDataTip
objs have a 'String'
%   property containing the data tip in the data tip's interpreter
format. When the
%   interpreter is converted to 'none', the PointDataTip string should
match the DataTip
%   content. This function uses the DataTip method when available or
the PointDataTip,
%   otherwise.
% [2] 'handle' can be a handle to a figure or axes and there are many
types of axes. This
%   method searches for membership of data tip handles to the
'handles' input whether
%   'handles' refers to a figure or axes no matter what axes type. If
'handles' is not a
%   figure or axes, due to user error, there will not be a membership.
% [3] Data tips in Matlab r2014a and earlier will not be identified by
the methods herein.
% [4] The parent for DataTips is the graphics object the data tip is
assigned to whereas
%   the parent for PointDataTips is the axes or group.

% Another way to get some of the data tip content is:
%       datacursormode on
%       dcmObj = datacursormode(gcf);
%       dcmStruc = getCursorInfo(dcmObj);
```

D.1.2. Convert Pixel Points

```
function [Timearr, Dataarr] = ConvertPixels(fig,
DataOrigin,PixelOrigin, MaxDataPt, MaxPicPt)
    %This function uses detected datatip points from a graph image and
    %converts them to usable datapoints

    %Requirement: Need the getDataTips function to function
```

```
    %Variables:
    %   fig: Figure handle you're passing to the function getDataTips.
    %   DataOrigin: Origin Point of the original data graph. Example:
(0,0)
    %   PixelOrigin: Pixel Origin location of the image figure.
Example: (1,1) for
    %   top left hand corner of the image (MATLAB Origin)
    %   MaxDataPt: Maximum datapoint value of the graph located in the
top
    %   right location. Example (10,100) for a graph with the max X =
10 and
    %   max Y = 100.
    %   MaxPicPt: Maximum pixel location on the bottom right location.
Example
    %   (1280,1080) for a 1080 p image

    %Determine the scaling factors for the image:
    Sx = (MaxDataPt(1)-DataOrigin(1))/(MaxPicPt(1)-PixelOrigin(1));
    Sy = (MaxDataPt(2)-DataOrigin(2))/(MaxPicPt(2)-PixelOrigin(2));

    %Detect the datatips for the graph image:
    Datatips = getDataTips(fig);

    %Make arrays to hold the pixel locations:
    Pixelt = zeros(1,length(Datatips{1})); %Time/X pixel data recorded
    Pixeld = zeros(1,length(Datatips{1})); %Data/Y pixel data recorded

    %String matrix of elements I don't need:
    match = ["X,Y", "[", "]", "]  "];

    for i = 1: length(Datatips{1})
        %Get the coordinate string out:
        Cdstr = Datatips{1}{i}(1);
        %Remove out the unused parts of this string:
        A = erase(Cdstr,match);
        %Get rid of the extra space at the beginning:
        B = A{1}(2:end);

        %Find where the space is between the numbers:
        Spind = find(isspace(B));

        %Store the data:
        Pixelt(i) = str2double(B(1:Spind-1)); %Time data
        Pixeld(i) = str2double(B(Spind+1:end)); %Quantity Data

    end
```

```
    %Convert the arrays of pixel X and Y locations to Time and Data
values
    Timearr = (Sx*Pixelt) + DataOrigin(1);
    Dataarr = Sy*(MaxPicPt(2)-Pixeld) + DataOrigin(2);

%     figure, plot(Timearr, Dataarr)
end
```

D.2 Validation Code

D.2.1 Central Derivative Function: MathWorks File Exchange (Mack, 2012)

```
function df = cent_diff_n(f,h,n)
% df = cent_diff_n(f,h,n)
% Computes an n-point central difference of function f with spacing h.
% Returns a vector df of same size as f.
% Input f must be a vector with evenly spaced points.
% Input n must be 3,5,7, or 9.
% All three inputs are required.
%
% Differences for points near the edges are calculated in lower order.
% For example, if n=5 and length(f)=10, then 3-point central
differencing is used
% to calculate values at points 2 and 9, 2-point forward differencing
is used for
% point 1, 2-point backward differencing is used for point 10, and 5-
point central
% differencing is used for points 3-7.
%
% If f contains less than n points, the order will be downgraded to
the
% maximum possible.  Ex: if length(f) = 6, n will be downgraded to 5.
%
% Differencing formulae from:
http://www.holoborodko.com/pavel/numerical-methods/numerical-
derivative/central-differences/
% Accessed 4/10/12.
%
% 4/10/12 (c) James F. Mack
if nargin < 3
    error('Not enough inputs.  See help documentation.')
end
if ~isscalar(h)
    error('Input h must be a scalar value.')
end
```

```
possible_ns = [3,5,7,9];
if ~ismember(n,possible_ns)
    error('Input n must be 3,5,7, or 9.')
end
numPts = length(f);
if numPts < n
    newN = max(possible_ns(possible_ns<=numPts));
    warnstr = [num2str(n) '-point differencing was requested,\n'...
       'but input function only has ' num2str(numPts) ' points.\n'...
       'Switching to ' num2str(newN) '-point differencing.'];
    warning(warnstr,'%s')
    n = newN;
end
df_1 = b_diff(f,h);
df_End = f_diff(f,h);
% Calculate 3-point for all
df_3pt = c_diff(f,h,3);
if n >=5
    df_5pt = c_diff(f,h,n);
    % For the 2nd and next-to-last grid point, use 3-point
differencing.
    df_2 = df_3pt(1);
    df_Endm1 = df_3pt(end);
end
if n >=7
    df_7pt = c_diff(f,h,7);
    % For the 3nd and 2nd from last grid point, use 5-point
differencing.
    df_3 = df_5pt(1);
    df_Endm2 = df_5pt(end);
end
if n>= 9
    df_9pt = c_diff(f,h,9);
    % For the 4nd and 3rd from last grid point, use 7-point
differencing.
    df_4 = df_7pt(1);
    df_Endm3 = df_7pt(end);
end
switch n
    case 3
        df = [df_1 df_3pt df_End];
    case 5
        df = [df_1 df_2 df_5pt df_Endm1 df_End];
    case 7
        df = [df_1 df_2 df_3 df_7pt df_Endm2 df_Endm1 df_End];
    case 9
```

```
        df = [df_1 df_2 df_3 df_4 df_9pt df_Endm3 df_Endm2 df_Endm1
df_End];
end

end
function df = c_diff(f,h,n)
midStartPoint = ceil(n/2); % First point at which full n points can be
used
midEndPoint = length(f)-midStartPoint+1; % Last point at which full n
points can be used
df = [];
for k = midStartPoint:midEndPoint
    switch n
        case 3
            df_k = (f(k+1) - f(k-1))/(2*h);
        case 5
            df_k = (f(k-2) - 8*f(k-1) + 8*f(k+1) - f(k+2))/(12*h);
        case 7
            df_k = (-f(k-3) + 9*f(k-2) - 45*f(k-1) + 45*f(k+1) -
9*f(k+2) + f(k+3))/(60*h);
        case 9
            df_k = (3*f(k-4) - 32*f(k-3) + 168*f(k-2) - 672*f(k-1) +
672*f(k+1) - 168*f(k+2) + 32*f(k+3) - 3*f(k+4))/(840*h);
    end
    df = [df df_k];
end
end
function df1 = b_diff(f,h)
df1 = (f(2)-f(1))/h;
end
function dfEnd = f_diff(f,h)
dfEnd = (f(end)-f(end-1))/h;
end
```

D.2.2 Beat-Per-Beat Summary Code

```
%% Beat-Per-Beat Summary and PV loop Datapoint Extraction:

%% Evenly Sample Datapoints from Simulink Simulation:
[Psanew,ty] = resample(PSA, tout);
LVPnew = resample(LVP, tout);
Folnew = resample(Fol, tout);
LVVnew = resample(LVV, tout);
Filnew = resample(Fil,tout);
dLVVdtnew = resample(Iheart,tout);
Planew = resample(LaP,tout);
```

```
HeartRatenew = HeartRate.*ones(length(tout),1);

%% Beat-Per-Beat Processing:

%Calculate the Numerical Derivative of LVP to get dP/dt:
dLVPn = cent_diff_n(LVPnew,mean(diff(ty)),3);

%Calculate the Derivative of Elastance:
dE = cent_diff_n(E1new,mean(diff(ty)),3);

%Calculate Cardiac Power:
CP = Psanew.*Folnew;

%Rising Edge and Falling Edge Detector for Resampled Flow out of Left
Ventricle (Folnew):
RE = zeros(1,length(Folnew));
FE = zeros(1,length(Folnew));

%Falling Edge Detector for Resampled Flow into the Left Ventricle
(Filnew):
RE_Fil = zeros(1,length(Filnew)-1);
FE_Fil = zeros(1,length(Filnew)-1);

%Detect Rising and Falling Edges of Fol waveform:
for i = 2: length(Folnew)-1
   if((Folnew(i)>0)&& (Folnew(i-1)==0))
      RE(i) = 1;
   end
    if((Folnew(i)>0)&& (Folnew(i+1)==0))
      FE(i) = 1;
   end
end

%Detect the Rising and Falling Edges of the Fil waveform:
for i = 1: length(Filnew)-1
   if((floor(Filnew(i))==0)&& (floor(Filnew(i+1))>0) &&
(floor(Filnew(i+2)>0)))
      RE_Fil(i) = 1;
   end
%     if((floor(Filnew(i))== 0)&& (floor(Filnew(i-1))> 0) &&
(floor(Filnew(i+1))== 0) && (floor(Filnew(i+2))== 0))
  if((Filnew(i)== 0)&& (Filnew(i-1)> 0) && (Filnew(i+1)== 0) )
     FE_Fil(i) = 1;
   end
end
```

```
%Detect Rising Edge Indicies for the Flow out of Left Ventricle (Fol):
RisingBeatnew = find(RE);
FallingBeatnew = find(FE);

%Detect Rising Edge Indicies for the Flow into the Left Ventricle
(Fil):
RisingBeatnew_Fil = find(RE_Fil);
FallingBeatnew_Fil = find(FE_Fil);

%Allocate memory for the Cardiac Power and Volume variables
CPb = zeros(1,length(RisingBeatnew)-1);
EDVb = zeros(1,length(RisingBeatnew)-1);
ESVb = zeros(1,length(RisingBeatnew)-1);
SVb = zeros(1,length(RisingBeatnew)-1);
EFb = zeros(1,length(RisingBeatnew)-1);
ESPb = zeros(1,length(RisingBeatnew)-1);
EDPb = zeros(1,length(RisingBeatnew)-1);
EDP_Aortab = zeros(1,length(RisingBeatnew)-1);
PulsePrb = zeros(1,length(RisingBeatnew)-1);
dPdtb = zeros(1,length(RisingBeatnew_Fil)-1);
SWb = zeros(1,length(RisingBeatnew)-1);
MAPb = zeros(1,length(RisingBeatnew)-1);
PEb = zeros(1,length(RisingBeatnew)-1);
Eesb = zeros(1,length(RisingBeatnew));
Effb = zeros(1,length(RisingBeatnew)-1);
EAb = zeros(1,length(RisingBeatnew)-1);
EA_EESb = zeros(1,length(RisingBeatnew)-1);
SW_PEb = zeros(1,length(RisingBeatnew)-1);
AvgLVPb = zeros(1,length(RisingBeatnew)-1);
%Cardiac Output:
COb = zeros(1,length(RisingBeatnew)-1);
%Heart Rate:
HRb = zeros(1,length(RisingBeatnew)-1);
%AoP:
AoPavgb = zeros(1,length(RisingBeatnew)-1);
AoPstdevb = zeros(1,length(RisingBeatnew)-1);
dE_maxb = zeros(1,length(RisingBeatnew)-1);

%Power and Work Done by the Left Heart
Powerb = zeros(1,length(RisingBeatnew)-1);
Workb = zeros(1,length(RisingBeatnew)-1);

%Counter to detect an iteration to break at:
counter = 1;

%Beat-per-Beat Processing Code:
```

```
for i = 1: index-1

    if (counter == (length(RisingBeatnew)-1 ))
        break;
    end

    %Increment the counter:
    counter =  counter +1;

    HRb(i) = mean(HeartRatenew(RisingBeatnew(i):RisingBeatnew(i+1)));

    %Determines the beat per beat EDV in ml/sec (Column B)
    EDVb(i) = max(LVVnew(RisingBeatnew(i):RisingBeatnew(i+1)));
    %Determines the beat per beat ESV in ml/sec (Column C)
    ESVb(i) = min(LVVnew(FallingBeatnew(i):FallingBeatnew(i+1)));
    %Determines the beat per beat SV in ml/sec (Column D)
    SVb(i) = EDVb(i)-ESVb(i);
    %Cardiac Output HR x SV (L/min):
    COb(i) = (SVb(i)* HRb(i))/1000;
    %Determines the beat per beat Ejection Fraction (Percent) (Column
E)
    EFb(i) = (SVb(i))./(EDVb(i));
    %Determines the ESPb per beat ESVb*(Max Elastance of LV per beat)
    %(Column F):
    ESPb(i) = LVPnew(FallingBeatnew(i));
    %End Diastolic Pressure (Column G)
    EDP_Aortab(i) = Psanew((FallingBeatnew_Fil(i)));
    %Pulse Pressure=Psa(systolic) - Psa(diastolic) (Column H):
    PulsePrb(i) = max(Psanew(RisingBeatnew(i):RisingBeatnew(i+1))) -
min(Psanew(RisingBeatnew(i):RisingBeatnew(i+1)));
    %Determines the dP/dt (i.e. dLVP/dt per beat) (Column I):
    dPdtb(i) =
max(dLVPn(RisingBeatnew_Fil(i):RisingBeatnew_Fil(i+1)));
    %Determines Mean Arterial Pressure
    MAPb(i) =
(sum(Psanew(RisingBeatnew(i):FallingBeatnew(i)))*mean(diff(ty)))/(ty(F
allingBeatnew(i))-ty(RisingBeatnew(i)));
    %Determines the SW = SV*MAP*0.0144 (g/m/m^2) (the area underne)
(Column J):
%   SWb(i) = SVb(i).*MAPb(i); %External Work
    %Mean LVP per beat:
    AvgLVPb(i) =
(sum(LVPnew(RisingBeatnew(i):FallingBeatnew(i)))*mean(diff(ty)))/(ty(F
allingBeatnew(i))-ty(RisingBeatnew(i)));
    SWb(i) = AvgLVPb(i).* SVb(i);
    %Determine the PE = 1/2*ESP*(ESV-uLVV) = 1/2*b*h (Column K):
```

```
    PEb(i) = (0.5.*ESPb(i).*(ESVb(i)- 16.77)); %in Joules
    %Determines the End Systolic Elastance (Column L): <-----(10
    %ms prior to dP/dt min)
    %Find location of minimum value of dP/dt during a beat within the
entire array of dLVP/dt:
    indexmin_dLVP = find(dLVPn ==
min(dLVPn(RisingBeatnew(i):RisingBeatnew(i+1))));
    %Go back 10 index locations to find value of elastance needed for
End
    %Systolic Elastance EES
    %Eesb(i) = Elastancenew(FallingBeatdelay_FOL(i)); %Old method
    Eesb(i) = E1new(indexmin_dLVP-10);

     %Determines the Efficiency per Beat (How much energy produced
out)/(Energy produced within the heart) (Column M):
    Effb(i) = (SWb(i))/(SWb(i)+PEb(i));
    %Determines the Effective Arterial Elastance (Column N):
    EAb(i) = ESPb(i)/SVb(i);
    %Determines EA/EES (Ratio looking at maximizing the area of the PV
loop) (Maximizing External Work Per Beat) (Column O):
    EA_EESb(i) = EAb(i)./Eesb(i);
    %Determines SW/PE (Column P):
    SW_PEb(i) = SWb(i)./PEb(i);
    %Determines the beat per beat cardiac power in Watts/sec (Column
Q)
    CPb(i) = mean(CP(RisingBeatnew(i):RisingBeatnew(i+1))*0.0001333);

    %Determine Power and Work:
    Powerb(i) =
mean(LVPnew(RisingBeatnew(i):RisingBeatnew(i+1)).*dLVVdtnew(RisingBeat
new(i):RisingBeatnew(i+1)));
    Workb(i) =
trapz(LVPnew(RisingBeatnew(i):FallingBeatnew(i)).*dLVVdtnew(RisingBeat
new(i):FallingBeatnew(i)));
    format long;
    MaxLVV = max(LVVnew(RisingBeatnew(i):RisingBeatnew(i+1)));
    MaxLVV = round(MaxLVV,3);
    for j = RisingBeatnew(i):RisingBeatnew(i+1)

%         if ((LVVnew(j-1)< MaxLVV) && (LVVnew(j) == MaxLVV) &&
(LVVnew(j+1)==MaxLVV))
%           if ((LVVnew(j-1)< MaxLVV) && (LVVnew(j+1)==MaxLVV))
          format long;
          point = round(LVVnew(j),1);
          pointback = round(LVVnew(j-1),1);
          pointforw = round(LVVnew(j+2),1);
```

```
%           if((pointback< point) && (Filnew(j+5) == 0) && (Filnew(j-
1) > 0))
          if((Filnew(j) == 0) && (Filnew(j+2) == 0) && (Filnew(j-1) >
0))
            EDPb(i) = LVPnew(j);
            EDP_Aortab(i) = Psanew(j);
          break;
          end
    end
    dE_maxb(i) = max(dE(RisingBeatnew(i):RisingBeatnew(i+1)));
end

%% Pick Points for Vena Caval Occlusion:

%First Select a Starting Time Point for Exporting to Excel:
figure, plot(ty,LVPnew), xlabel('Time'), ylabel('LVP');

[x1, ~] = ginput(2);

P1 = x1(1);
P2 = x1(2);

disp('You picked point 1 at: ');
disp(P1);
disp('You picked point 2 at: ');
disp(P2);

if(P2 <  P1)
        Temptime = P2;
        P2 = P1;
        P1 = Temptime;
end
if(P1 == 0)
    P1 = 1;
end
if(P2 == 0)
    P2 = 1;
end
[~,Ind1] = min(pdist2(P1,ty));
[~,Ind2] = min(pdist2(P2,ty));

%Find the beat number used for exporting the data:
cP1 = interp1(RisingBeatnew,RisingBeatnew,Ind1,'nearest'); %Closest
point to the index 1
B1 = find(RisingBeatnew == cP1)
```

```
cP2 = interp1(RisingBeatnew,RisingBeatnew,Ind2,'nearest'); %Closest
point to the index 2
B2 = find(RisingBeatnew == cP2)

%Get the distance of the points for export:
distance = length(B1:B2);

%% Get the Title that the user wishes to export with:
%Export to Excel:
%Ask user for input:
prompt = 'Enter in the Type of Simulation:  ';
xsummary = input(prompt,"s");
filename = sprintf('Simulink Beat Per Beat Summary data for %s.xlsx',
xsummary);
```

D.2.3 Segment PV Datapoints into Segmented Loops

```
%% Segment the PV Loops for Excel Sheet

%Make a matrix to hold the PV loop data:
format short
%Check the sizes of the points:
SizeArr = zeros(1,distance);

for i = 0:distance-1

    %disp(['The length of Beat', num2str(P1+i),' LVV and LVP'])
    LVVlength =
length(LVVnew(RisingBeatnew_Fil(B1+i):RisingBeatnew_Fil(B1+1+i)));
    LVPlength =
length(LVPnew(RisingBeatnew_Fil(B1+i):RisingBeatnew_Fil(B1+1+i)));

    SizeArr(i+1) = min(LVVlength,LVPlength);

end


MaxLength = max(SizeArr);

PVdata = NaN(MaxLength, 2*distance);
BeatPVmat = cell(1,2*distance);
SignalPVmat = cell(1,2*distance);

Beatnum = cell(1,distance);

figure();
```

```
for i = 0:distance-1

   Pstart = B1+i;
   Pend = Pstart+1;

   BeatPVmat{1,(2*i)+1} = strcat('Beat', ' ', num2str(Pstart));
   SignalPVmat{1,(2*i)+1} = strcat('LVV', ' ',num2str(Pstart));
   SignalPVmat{1,(2*i)+2} = strcat('LVP ', ' ',num2str(Pstart));

   %Get the Iteration Array Needed for PV Loops
   LVVmat =
[LVVnew(RisingBeatnew_Fil(Pstart):RisingBeatnew_Fil(Pend))];
   LVPmat =
[LVPnew(RisingBeatnew_Fil(Pstart):RisingBeatnew_Fil(Pend))];
   %Get the Length:
   LengthLVV = length(LVVmat);
   LengthLVP = length(LVPmat);


   PVdata(1:LengthLVV,(2*i)+1) = LVVmat;
   PVdata(1:LengthLVP,(2*i)+2) = LVPmat;


   plot(LVVmat, LVPmat), hold on;
   Beatnum{i+1} = strcat('Beat ',num2str(1+i));
end

title('Segmented PV Loops during Vena Caval Occlusion')
xlabel('Left Ventricular Volume')
ylabel('Left Ventricular Pressure')
legend(Beatnum)

% Remove any zeros with NaN
PVdata(PVdata == 0) = NaN;
```

D.2.4 Export to Excel

```
%% Create the matrixes for the combined data
DataMatrix =
[(B1:B2)',HRb(B1:B2)',EDVb(B1:B2)',ESVb(B1:B2)',EFb(B1:B2)',SVb(B1:B2)
',...

COb(B1:B2)',ESPb(B1:B2)',EDPb(B1:B2)',EDP_Aortab(B1:B2)',PulsePrb(B1:B
2)',dPdtb(B1:B2)',....
    SWb(B1:B2)', PEb(B1:B2)', Eesb(B1:B2)', Effb(B1:B2)', EAb(B1:B2)',
EA_EESb(B1:B2)',...
```

```
    SW_PEb(B1:B2)', CPb(B1:B2)',
dE_maxb(B1:B2)',Powerb(B1:B2)',Workb(B1:B2)'];

DataMatrix = round(DataMatrix,2);

%LVP and LVV Data for PV Loops:
PVLoops = [LVVnew(Ind1:Ind2),LVPnew(Ind1:Ind2)];

%Make a Title Matrix:
Titles = {'Beat', 'Heart Rate','EDV','ESV','EF','SV','Cardiac
Output','ESP','EDP','EDP of Aorta',...
    'Pulse Pressure','dP/dt','SW','PE',
'EES','EFF','EA','EA/EES','SW/PE','Cardiac Power','dEmax',...
    'Left Ventricular Power', 'Left Ventricular Work'};
%Get the Averages and Standard Deviation for Excel Sheet:
AverageData = num2cell(mean(DataMatrix(:,2:end)));
StdevData = num2cell(std(DataMatrix(:,2:end)));

%Make Cell matrix to Hold Title for Bottom Row:
Avgmat = {'Average'};
Stdevmat = {'Standard Deviation'};

Avgmat = cat(2, Avgmat, AverageData);
Stdevmat = cat(2,Stdevmat, StdevData);
%Concatenate the Titles on Top of the Combined Data:
ExportMatrix = cat(1,Titles, num2cell(DataMatrix), Avgmat, Stdevmat);

%Save to a .mat file for future processing:
save(strcat(xsummary,'.mat'),'ExportMatrix')
save(strcat(xsummary,'Selected PV Loops.mat'),'PVdata')

writecell(ExportMatrix,filename,'Sheet',1,'Range','A1');
writecell(BeatPVmat,filename,'Sheet',2','Range','A1');
writecell(SignalPVmat,filename,'Sheet',2','Range','A2');
writecell(num2cell(PVdata),filename,'Sheet',2,'Range','A3');
```

APPENDIX E: CONTACT INFORMATION TO REQUEST ACCESS TO THE SIMULINK MODEL

Please contact by email at julian.thrash@ndsu.edu or julian.e.thrashiii@gmail.com to request access to the Simulink Cardiopulmonary model repository on GitHub. You will be asked to sign a non-disclosure and competition agreement prior to getting access to the model.